

DEVELOPMENT OF A HYPOXIA ACTIVATED PRODRUG FOR THE SELECTIVE  
INHIBITION OF DNA-DEPENDENT PROTEIN KINASE

by

JORDAN DARICE CRAN

B.Sc., Simon Fraser University, 2010

A THESIS SUBMITTED IN PARTIAL FULFILLMENT OF THE REQUIREMENTS FOR  
THE DEGREE OF

MASTER OF SCIENCE

in

THE FACULTY OF GRADUATE STUDIES

(Pathology & Laboratory Medicine)

THE UNIVERSITY OF BRITISH COLUMBIA

(Vancouver)

April 2013

© Jordan Darice Cran, 2013

## Abstract

The presence of tumour hypoxia, regions of low levels of oxygen, is a distinct and exploitable feature of the solid tumour microenvironment. While its presence is generally accepted as a negative prognostic indicator, hypoxia is a relatively unique feature to solid tumours and can therefore be exploited as a means to specifically target cancer cells in this setting. Prodrugs can be designed to harness the reductive environment found within hypoxic cells, by releasing an active drug following reduction. This work continues the development of a prodrug, Hapi3, which under hypoxic conditions releases an inhibitor of the DNA-dependent protein kinase (DNA-PK). DNA-PK is the central component to the non-homologous end joining pathway (NHEJ) used to repair double strand breaks and base damage induced by ionizing radiation (IR). Inhibition of repair within hypoxic environments in conjunction with IR provides a means to selectively target tumour cells. Previously, clonogenic survival was used to determine that Hapi3 provides a sensitization enhancement ratio of 1.8 and does not release the active inhibitor, IC86621, under normoxic conditions. The objective of this research is to evaluate formulations of Hapi3 in mice to achieve desirable tissue concentrations for radiosensitization and perform efficacy studies to determine if hypoxic inhibition of repair will improve the efficacy radiation therapy in an *in vivo* tumour model. Due to Hapi3 solubility limitations, the dose necessary to achieve radiosensitization in tissues was not achieved as evidenced by a lack of observable growth delay. Compounds based on IC86621 are unsuitable for further development, however syntheses of new hypoxia activated repair inhibitors should be pursued.

## Preface

This thesis has been prepared in partial fulfillment of the requirement for the degree of Master of Science in Pathology and Laboratory Medicine. I have prepared this thesis in its entirety under the direction and supervision of Dr. Andrew Minchinton. This thesis was revised by Dr. Andrew Minchinton, Dr. Jennifer Baker and Kirstin Lindquist.

This thesis is an investigation into the *in vivo* efficacy of the hypoxia activated DNA-dependent protein kinase inhibitor Hapi3 lead by Dr. Minchinton. Formulation of Hapi3 was the result of extensive collaboration with Dr. Norbert Maurer, head of Formulation at the Centre for Drug Research and Development (UBC). Members of the Maurer laboratory, namely Matthew Wong and Carlos Fleet, were responsible for preparing various formulations of Hapi3 for tolerability and efficacy testing. The Maurer lab conducted initial solubility and dissolution screening, guided the development of and prepared all formulations. I was responsible for developing an assay to quantitate Hapi3 in murine tissue, evaluating different Hapi3 formulations by microscopy and planning, as well as conducting *in vivo* tolerability, toxicity and efficacy studies in mice. Analysis of the research data was conducted by myself and members of the Minchinton laboratory.

This study was approved the by the Animal Care Committee of University of British Columbia (A09-0265) and was carried out in strict accordance with standards and guidelines put forth by the Canadian Council on Animal Care (CCAC).

# Table of Contents

Abstract.....	ii
Preface .....	iii
Table of Contents.....	iv
List of Tables .....	vii
List of Figures.....	viii
Glossary .....	ix
Acknowledgements.....	xi
Dedication .....	xii
Chapter 1: Introduction.....	1
1.1 Hypothesis and specific aim .....	1
1.2 Radiation and the oxygen effect.....	2
1.3 Hypoxia and the solid tumour microenvironment.....	5
1.4 DNA damage response in eukaryotic cells .....	8
1.5 Repair inhibitors .....	12
1.6 Hypoxia activated prodrugs .....	14
1.7 Formulation of insoluble drugs.....	16
Chapter 2: Materials and methods .....	18
2.1 Inhibitor and prodrug.....	18
2.2 High pressure liquid chromatography .....	18
2.3 Cell culture .....	18
2.4 Resazurin assay .....	19
2.5 Radiation treatment.....	20
2.6 Prodrug formulation .....	20



2.7 Blood and tissue sample collection and processing .....	22
2.8 In vivo efficacy studies .....	22
2.9 Statistical analysis.....	23
Chapter 3: High pressure liquid chromatography assay to quantitate Hapi3 .....	24
3.1 Assay validation .....	24
Introduction.....	24
Approach .....	24
Results and Discussion .....	25
3.2 Sample matrix effects and recovery from tissue .....	26
Introduction.....	26
Approach .....	26
Results and Discussion .....	27
Chapter 4: Hapi3 formulation for in vivo studies.....	30
4.1 Formulation of Hapi3 with block copolymers and milling .....	30
Introduction.....	30
Approach .....	31
Results and Discussion .....	32
Chapter 5: Biodistribution and efficacy testing .....	38
5.1 DNA-PK inhibition sensitizes H460 and SCCVII cells to ionizing radiation in vitro .....	38
Introduction.....	38
Approach .....	39
Results and Discussion .....	40
5.2 Concentration of Hapi3 in blood plasma and biodistribution studies .....	44
Introduction.....	44

Approach .....	44
Results and Discussion .....	45
5.3 In vivo efficacy studies .....	50
Introduction.....	50
Approach .....	50
Results and Discussion .....	51
Chapter 6: Conclusions and future work .....	56
References .....	60
Appendices.....	69

## List of Tables

Table 3.1 Slope, intercept and determination coefficient of regression equations resulting from Hapi3 calibration curves .....	27
Table 3.2 Average extraction efficiency of Hapi3 in plasma and tissues.....	30
Table 5.1 Average tissue concentration of Hapi3 6 h post gavage .....	49
Table of DNA-PK inhibitors.....	70

# List of Figures

Figure 1.1 Chemical structures of prodrug Hapi3 and DNA-dependent protein kinase inhibitor IC86621 .....	1
Figure 1.2 DNA damage from ionizing radiation.....	3
Figure 1.3 Hypoxic cells are resistant to ionizing radiation.....	5
Figure 1.4 Survival probabilities of patients with locally advanced cancer of the uterine cervix treated with radiotherapy ± chemotherapy stratified for tumour oxygenation.....	7
Figure 1.5 Model of non-homologous end joining .....	11
Figure 1.6 Typical prodrug mechanism with nitroaromatic linker.....	15
Figure 3.1 Hapi3 calibration curve constructed with external standards of Hapi3 in methanol/6% ZnSO <sub>4</sub> .....	25
Figure 3.2 Tissue calibration curves constructed using HPLC analysis of Hapi3 added to tissue homogenates .....	29
Figure 4.1 Solutol® HS-15 structure .....	34
Figure 4.2 Brightfield microscopy of Hapi3 crystalline suspensions.....	35
Figure 4.3 Brightfield microscopy of Hapi3 crystalline polymer suspensions.....	36
Figure 4.4 Brightfield microscopy of ball-milled Hapi3 crystalline suspensions .....	37
Figure 5.1 Reduction of resazurin to resorufin.....	39
Figure 5.2 Effects of DNA-PK inhibition by IC86621 in combination with radiation in HCT116 cells .....	42
Figure 5.3 Effects of DNA-PK inhibition by IC86621 in combination with radiation in murine SCCVII cells .....	43
Figure 5.4 Concentration of Hapi3 in plasma following oral gavage .....	48
Figure 5.5 Hapi3 in muscle tissue following oral administration .....	49
Figure 5.7 Hapi3 provides no significant additional growth delay over radiation alone	54
Figure 5.8 in vivo toxicity evaluated by body weight loss .....	55

# Glossary

$\lambda$	Light wavelength
$\mu\text{mol}$	Micromole
$\mu\text{g}$	Microgram
$\mu\text{L}$	Microlitre
AUC	Area under the curve
cm	Centimetre
C <sub>max</sub>	Maximum concentration of a drug in the body or blood following administration
d	Days
DDR	DNA damage response
DNA	Deoxyribonucleic acid
DNA-PK	Deoxyribonucleic acid dependent kinase
DNA-PKcs	Deoxyribonucleic acid dependent kinase catalytic subunit
DMSO	Dimethyl sulfoxide
DSB	Double strand break
Gy	Gray
h	Hours
HAP	Hypoxia activated prodrug
HR	Homologous recombination
IR	Ionizing radiation
i.v.	Intravenous
i.p.	Intraperitoneal
kg	Kilogram
LOD	Limit of detection
LOQ	Limit of quantitation
MEM	Minimal essential media

min	Minutes
mg	Milligrams
mL	Millilitre
mm	Millimetre
Morpholine	A heterocyclic chemical compound with the formula $O(CH_2CH_2)_2NH$
NHEJ	Non-homologous end joining
nm	Nanometre
PARP	Poly ADP ribose polymerase
PDA	Photodiode array
PEG	Polyethylene glycol
PFGE	Pulse field gel electrophoresis
PI3K	Phosphatidylinositol 3 kinase
RPA	Replication protein A
SEM	Standard error of the mean
SER	Sensitization enhancement ratio
SSB	Single strand break
ssDNA	Single strand DNA
THF	Tetrahydrofuran

## Acknowledgements

First and foremost, I would like to thank my supervisor Dr. Andrew Minchinton for giving me the opportunity to pursue graduate studies. Thank you to my lab mates, Dr. Alastair Kyle for building such wondrous equipment and answering so many questions; Dr. Jennifer Baker for her insight, honesty and generosity of time; Maria Jose Gandolfo, for countless hours of experimental and technical support; Tania Karan for her humor, relentless grammar and endless optimism; I am especially grateful to Kirtsin Yuzwa for her mentorship, support and encouragement. Thank you to our chemically inclined collaborators Matt Smith, Carlos Fleet and Dr. Norbert Maurer.

Thank you to my supervisory committee Drs. Marcel Bally, Kishor Wasan, Paul Rennie, your perspective and advice has been invaluable. Thank you to Wil Cottingham for your help and support, as well as to 9th floor at BC Cancer Research Centre for general support and friendship.

To Natalie Taha for her love, example, spirit, her kitchen table at times and so much else. For pulling me through my undergrad and pushing me through my graduate work. I could not ask for or find a truer friend.

Thank you to my partner Richard Gosse for your patience, love, support, and laughter; Also the entire Gosse family for welcoming me into their hearts and home.

## Dedication

I would like to take this opportunity to dedicate this work to my immediate family, and *most especially to my mother, Gay*. Thank you for your unwavering support of my education and unconditional love, without it this work would not be possible. Your strength, endurance, courage and perseverance have inspired and helped shape the person I am today and the person I will become in the days and years that follow.



# Chapter 1: Introduction

## 1.1 Hypothesis and specific aim

Previously candidate prodrugs synthesized by members of Dr. Gregory Drake's laboratory at the UBC Department of Chemistry were tested for hypoxia specific activity by Kirstin Lindquist in the Dr. Andrew Minchinton's laboratory as part of her Masters thesis project (1). Prodrugs were modeled after the DNA-dependent protein kinase (DNA-PK) inhibitor IC86621 as it contained a suitable functional group (phenolic hydroxyl) for conjugation to the prodrug moiety. Hapi3 emerged as the most promising candidate for further development. Structures of Hapi3 and IC86621 are shown in Figure 1.1. Minchinton et al. (unpublished data) determined by *in vitro* clonogenic survival assays that the prodrug provided hypoxia specific radiosensitization in several carcinoma cell lines. Suspensions of either mouse liver microsomes or stirred cells showed release of IC86621 from Hapi3 to be an NADPH dependent process, with efficient release occurring at oxygen tensions  $\leq 1\%$  O<sub>2</sub>.

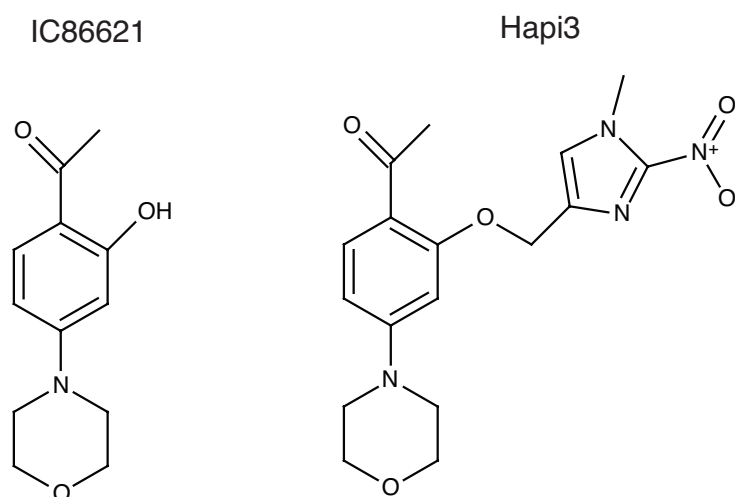


**Figure 1.1 Chemical structures of prodrug Hapi3 and DNA-dependent protein kinase inhibitor IC86621**

The **hypothesis** of my thesis is that *hypoxia selective inhibition of the DNA-dependent protein kinase will sensitize radiation resistant hypoxic cells in vivo and provide better growth delay following radiation therapy*. The following specific aims will address my hypothesis:

1. To develop an assay to quantitate Hapi3 in tissues and determine if Hapi3 can be reliably quantified by HPLC.
2. To determine if formulation approaches can increase the bioavailability of crystalline suspensions of Hapi3.
3. To determine if administration of a hypoxia activated DNA-PK inhibitor can sensitize solid tumours to radiotherapy in an *in vivo* mouse model.

## **1.2 Radiation and the oxygen effect**

Radiation therapy is an essential component of cancer therapy. An estimated 50 % of all newly diagnosed cancer patients will receive radiation therapy at some point during treatment (2). The technological advances of the last 20 - 30 years have greatly improved the accuracy of dose delivery to diseased tissue, thereby allowing for increases in dose to the tumour and a reduction in dose to surrounding normal tissue (3). Despite improvements in dose deposition many patients are still afflicted by locally recurrent disease (4), emphasizing the need to continue to improve tumour cell kill from ionizing radiation (IR).

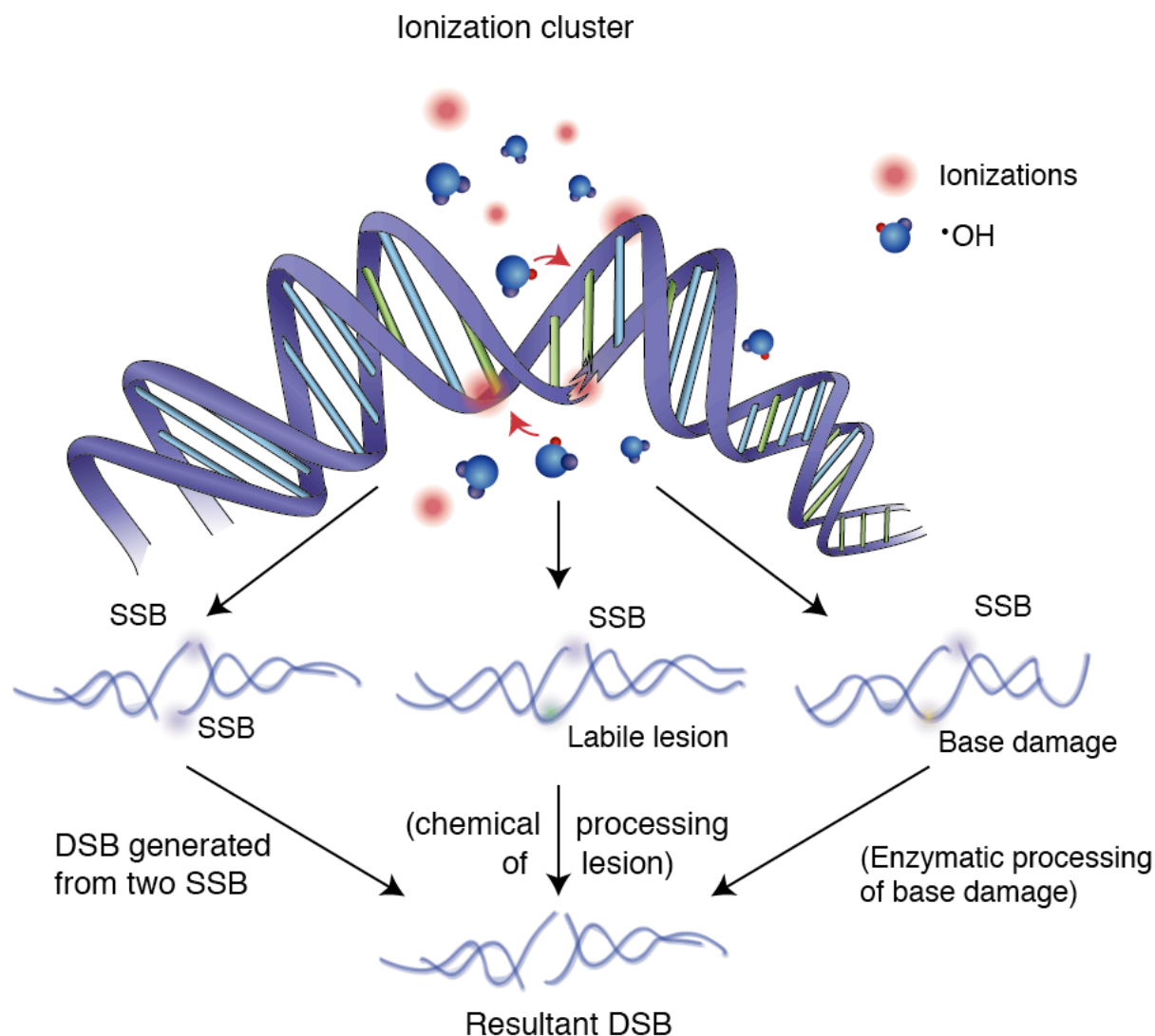


**Figure 1.2 DNA damage from ionizing radiation**

Charged particles interact with DNA directly, damaging the DNA molecule by depositing energy, resulting in ionization from loss of an electron. The interaction of charged particles with the solvation shell surrounding DNA results in the generation of other free radical species, namely the hydroxyl radical. This indirectly results in further DNA damage owing to the proximity of the free radicals species to DNA and their chemical instability. Direct and indirect damage results in a wide variety of complex lesions consisting of combinations of single strand breaks and damage to the bases or phosphate backbone. Processing of this damage by the cellular repair machinery often results in double strand breaks (DSBs) and loss of genetic information. Reprinted from *Mutational Research*, vol. 711/1-2, Mladenov, E. and Iliakis, G., Induction and repair of DNA double strand breaks: The increasing spectrum of non-homologous end joining pathways, pp 61 - 72, Copyright (2011), with permission from Elsevier.

The biological effects of IR primarily result from its interaction with DNA. While DNA is not the sole molecule damaged by radiation, it is of greatest importance when considering cell survival. Damage to DNA can be both direct and indirect. The direct interaction of high energy photons with DNA results in the excitation and ionization of DNA, forming DNA radical species. The indirect damage to DNA results from radiolysis of water (5). Absorption of photon energy by water molecules surrounding DNA results in water radiolysis, forming three major radical species,  $\text{OH}\cdot$ ,  $\text{H}\cdot$  and  $\text{e}_{\text{aq}}^-$ . These radical species are able to diffuse short distances, interact with and damage DNA (6). The direct effects account for approximately 35% of damage incurred by radiation, while indirect effects from radicals account for the remaining 65% (7). The formation of multiple lesions within one helical turn of DNA, affecting both strands, is commonly referred to as complex or clustered DNA damage and is a unique feature of IR and is summarized in Figure 1.2 (8). According to the *oxygen fixation hypothesis*, DNA radicals may undergo oxidation by molecular oxygen resulting in the formation of an organic peroxide, a non-restorable form of DNA damage (9). However under hypoxic conditions, when oxygen is scarce, chemical restitution of the DNA to its original form by thiol containing compounds within the cell may occur, resulting in radiation resistance (10,11); This phenomenon is commonly referred to as the oxygen effect.

Evidence for the oxygen effect is illustrated in a cell-survival curve shown in Figure 1.3 which quantitatively shows that in the absence of oxygen, cells require a 2.5 - 3.0 increase in dose to achieve the same surviving fraction as cells in the presence of oxygen (12-15). Although technical advances in treatment planning and delivery have improved treatment, the resistance of hypoxic cells to IR remains one of the major

hurdles in radiotherapy today. Despite the overwhelmingly negative role of hypoxia in radiation therapy, hypoxia is a unique feature of solid tumours (discussed below) relative to most normal physiological conditions found in the human body, and may therefore be considered therapeutically exploitable.

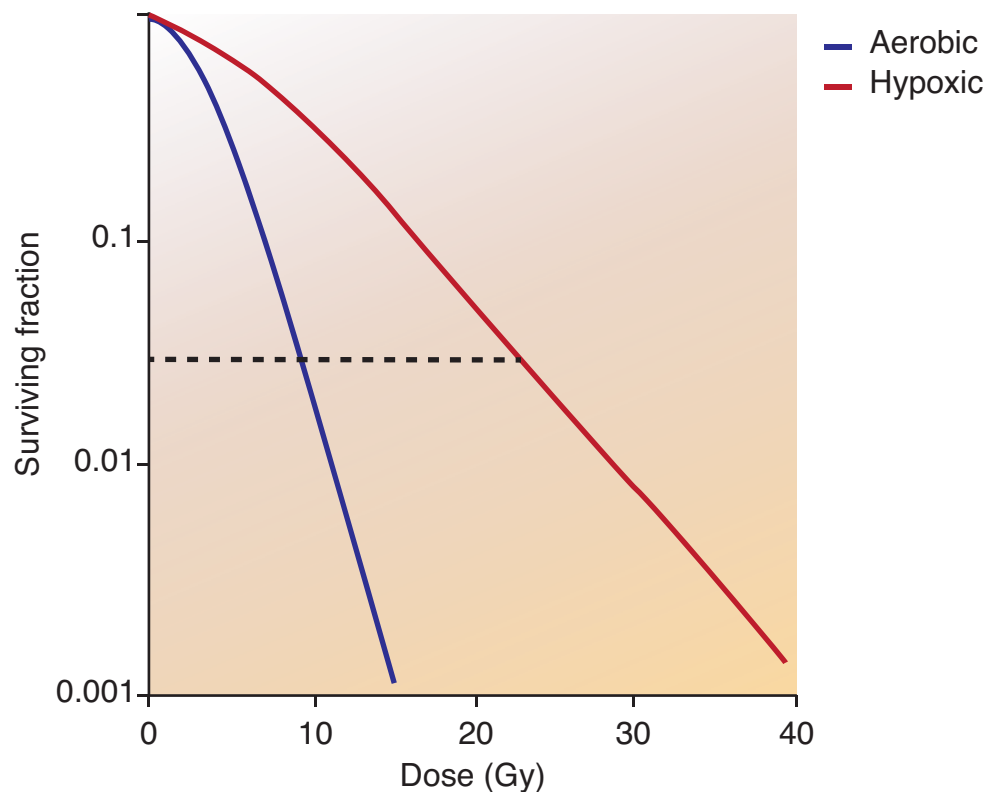


**Figure 1.3 Hypoxic cells are resistant to ionizing radiation**

Typical cell-survival curves illustrate the effect of oxygen in sensitizing cells to IR. The oxygen enhancement ratio (OER) is defined as ratio of dose required to produce an equivalent surviving fraction of hypoxic cells to aerobic cells (see dashed line). Hypoxic cells are on average 2 - 3 times more resistant to the effects of IR than aerobic cells (12,13). Adapted by permission from Macmillan Publishers Ltd: Nature Reviews Cancer (15), copyright 2004.

### 1.3 Hypoxia and the solid tumour microenvironment

It is now well established that hypoxia is a common feature of the solid tumour microenvironment which has great influence on response to therapy. However, the relationship between oxygen tension and sensitivity to IR in tumours was only first

demonstrated by Gray and colleagues in the early 1950s (14). Thomlinson and Gray (1955) observed what is now defined as chronic hypoxia; large areas of necrosis separated from blood vessels or stroma by bands of tumour cells 100 - 150  $\mu\text{m}$  wide (16). The authors showed that this distance corresponds to the oxygen diffusion distance when taking into account the rate of oxygen consumption by cells and the partial pressure of oxygen ( $\text{pO}_2$ ) in surrounding capillaries. Owing to the quiescent state and distal location of chronically hypoxic cells from blood vessels, these cells exhibit resistance to many chemotherapeutic agents as well (17-19). Hypoxia may also be acute or perfusion limited (20-22). The insufficient delivery of oxygen and nutrients to tissues characterizes acute hypoxia and is the result of the poor organization and compromised structure of tumour vasculature (23,24).

Work by Gray and colleagues provided key empirical data indicating tissue oxygenation status as a key factor in the response to IR, however little in the way of clinical evidence was possible for several decades(14,16). The negative prognostic effects of hypoxia on radiotherapy in clinical patients became available in the early 1990s with the invention of the Eppendorf oxygen electrode (25-27). The electrode, embedded within a needle for insertion into tissue, uses polarography to measure oxygen tension within the tissue. Moeller *et al.* (2007) have summarized the major studies examining  $\text{pO}_2$  in tissues, illustrating hypoxia as a negative prognostic indicator for cervical and head and neck carcinomas, as well as soft tissue sarcomas treated with radiation therapy (28). Results from a representative study are shown in Figure 1.4. Significantly shorter survival was observed in patients bearing tumours with median  $\text{pO}_2 \leq 10 \text{ mm Hg}$ .

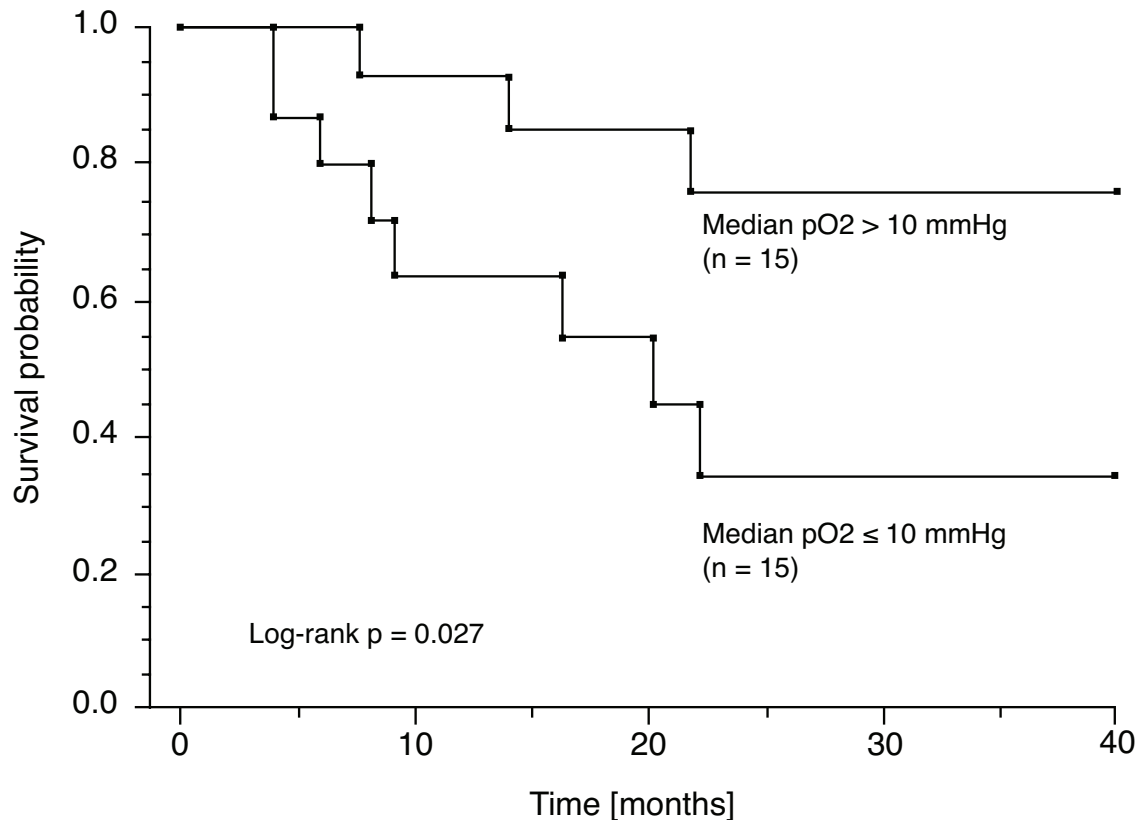


**Figure 1.4 Survival probabilities of patients with locally advanced cancer of the uterine cervix treated with radiotherapy ± chemotherapy stratified for tumour oxygenation.**

Median measurements obtained with the Eppendorf oxygen electrode allowed for stratification of patients based on tumour pO<sub>2</sub> measurements. Patients with tumours exhibiting average pO<sub>2</sub> measurements ≤ 10 mmHg had significantly shorter survival compared with patient tumours with median pO<sub>2</sub> > 10 mm Hg. Reprinted from *Gynecologic Oncology*, vol. 51 (2), Höckel et al., Tumor oxygenation: a new predictive parameter in locally advanced cancer of the uterine cervix, pp 141 - 149, Copyright 1993, with permission from Elsevier.

Hypoxic cells exhibit resistance to other forms of therapy as well. Many anti-cancer drugs act by damaging DNA or interfering with critical cell functions and as such produce the greatest effect in rapidly proliferating cells (29-31). As hypoxia is a relatively unique feature of the solid tumour microenvironment, it could be exploited for therapeutic gain (32).

Initial attempts to overcome the “hypoxia problem” included small molecule hypoxic radiosensitizers, hyperbaric oxygen and RT with heavy nuclear particles (33). Small molecule nitroaromatic compounds, nitroimidazoles, were reported as potent hypoxic cell radiosensitizers (33,34). Compared with oxygen, nitroimidazoles are less rapidly consumed while diffusing out of blood vessels and through tumour tissue, allowing these drugs to reach chronically hypoxic tumour cells that exist beyond the diffusion distance of oxygen (33,35,36). Meta-analysis by Overgaard *et al.* (1996) examining trials conducted between 1970 - 1998 indicated that a significant benefit in loco-regional control was observed for individuals with squamous cell carcinoma of the head and neck who received hypoxic modification of radiotherapy (hyperbaric oxygen or hypoxic sensitizers)(37).

#### **1.4 DNA damage response in eukaryotic cells**

The cellular DNA damage response (DDR) involves the coordination of a complex set of signaling processes encompassing multiple DNA damage detection and repair pathways. Ultimately this response results in cell survival or cell death depending on the extent of the damage and if the damage can be repaired. While radiation induces a variety of lesions, DNA double strand breaks (DSBs) are considered most lethal (38-40). DSBs are predominately repaired by two pathways, homologous recombination (HR) and non-homologous end joining (NHEJ) (8,41,42).

HR is considered a higher fidelity processes as it uses a complimentary strand of DNA to conserve DNA sequence at the lesion site, however HR is restricted to late S and G2 phases of the cell cycle when sister chromatids are present. Following end processing,



HR is thought to proceed in three distinct phases: presynaptic filament formation, synapsis and post synaptic strand exchange/branch migration. Subsequently the two broken ends are annealed and the double Holliday junction is resolved by other protein complexes within the cell.

NHEJ is the predominant pathway for repair of DSBs in mammalian cells and is accomplished through the joining and ligation of two free ends of DNA, with little or no homology required (43,44). The serine/threonine DNA-dependent protein kinase (DNA-PK) is a central component of NHEJ and is composed of the catalytic subunit DNA-PKcs and the Ku heterodimer, consisting of Ku70 and Ku86 (also referred to as Ku80). Due to the relative abundance of Ku (~ 400,000 molecules per cell) and its high binding affinity for the ends of double strand DNA, Ku is thought to be the first protein to bind the ends of DSBs (45,46). Ku encircles the ends of double-strand DNA in a sequence independent manner by forming an asymmetric ring which interacts with the sugar phosphate backbone and allows for recruitment of DNA-PKcs and subsequent activation of the kinase domain by autophosphorylation (47). Activation of the kinase domain is a critical component of NHEJ and is required for the successful completion of NHEJ (48-52).

Owing to the complex and highly variable nature of IR induced breaks, processing of damage to the sugar-phosphate backbone or bases may require substantial deletions or additions of nucleotides to restore molecular integrity (Figure 1.5). End processing factors required include various exonucleases, polymerases and ligases reviewed in detail by Lieber (2010) (53). Mladenov *et al.* (2011) note that as yet, no mechanism has

been discovered which ensures that the original ends will be rejoined, providing a possible mechanism for translocations which may contribute to carcinogenesis (8).

Due to the central role of DNA-PK in NHEJ, inhibition of the kinase domain is an attractive therapeutic target. While the component of NHEJ would still be recruited to DSB sites, inhibition of autophosphorylation retards the dissociation of DNA-PKcs and prevents the timely completion of NHEJ as well as access to the DNA end. Commonly used chemotherapeutics, such as alkylating agents, topoisomerase I and II inhibitors, and anti-metabolites are known or suspected to induce DSBs. Therefore, inhibiting repair in cancer cells would not only potentiate IR induced lesions but DNA damage from chemotherapy as well. Increasing the efficacy of chemotherapeutic agents and IR would mean lower doses would be required to achieve the same therapeutic effect, thereby reducing toxicity for normal tissues.

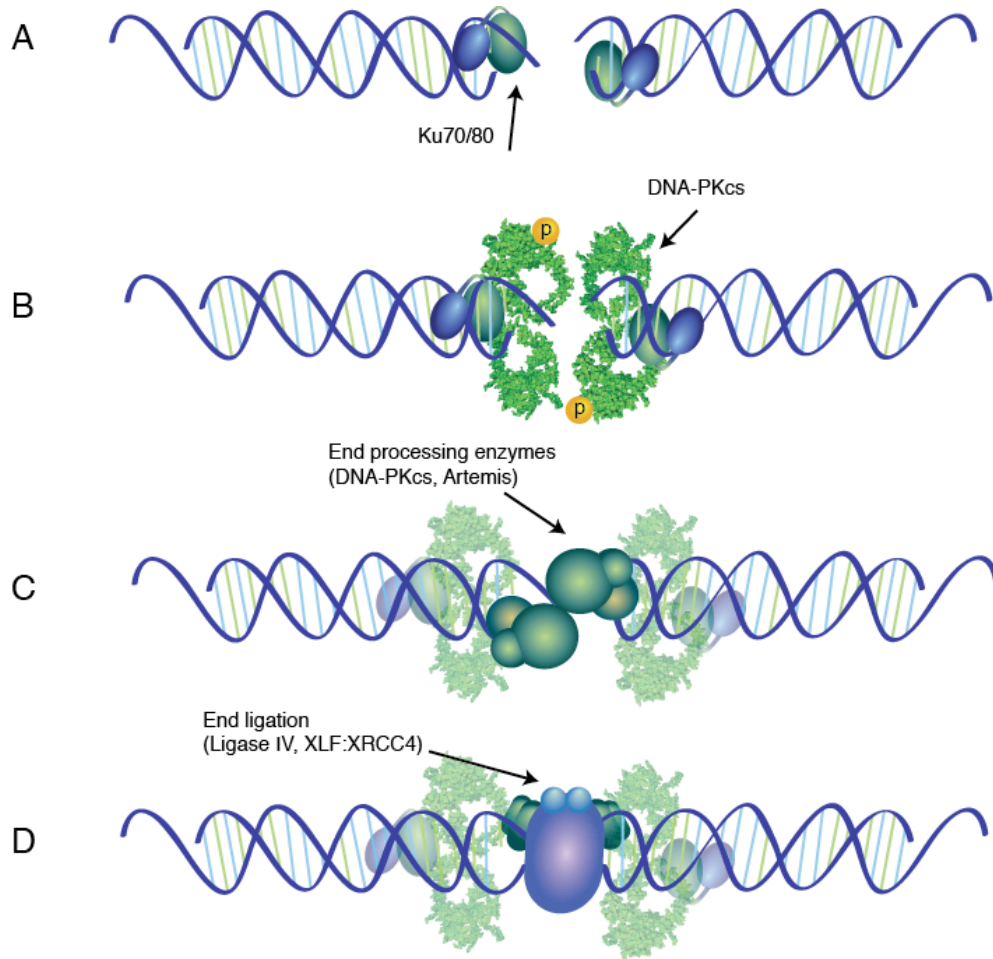


**Figure 1.5 Model of non-homologous end joining.**

A) Following induction of a DSB, the Ku70/80 heterodimer bind the broken ends of DNA. Acting as a scaffold, the Ku-DNA allows the binding of catalytic subunit, DNA-PKcs, forming a synaptic complex. B) The kinase ability of DNA-PK becomes activated following binding to the DSB, and allows for autophosphorylation of DNA-PKcs, an essential step for efficient completion of NHEJ ((54). C) Incompatible DNA termini require processing before subsequent ligation and restoration of molecular integrity. Polymerases and exonucleases add or resect nucleotides to facilitate D) ligation of termini by the Ligase IV:XLF:XRCC4 complex.

## 1.5 Repair inhibitors

Targeting DNA repair pathways in cancer treatment is a promising approach for improving the efficacy of many conventionally used therapies. Through the selective inhibition of repair the efficacy of current DNA damaging therapies can be greatly improved. A review by Helleday *et al.* (2008) describes how the inhibition of individual repair pathways can increase the potency of complimentary DNA damaging agents, including IR(55). Reviewed here are studies which successfully used inhibition of DSB repair to enhance the efficacy of DNA damaging modalities.

PI3K inhibitors wortmannin and LY294002 were early candidates as radiosensitizers. Despite effective *in vitro* radiosensitization, both compounds produced unacceptable toxicity in animals and presented considerable formulation or pharmacokinetic and pharmacodynamic challenges (56-58). Structurally similar to LY294002, potent DNA-PK inhibitor NU7026 produced significant radiosensitization in murine embryonic fibroblasts and Chinese hamster cells *in vitro* (59,60). However, *in vivo* pharmacokinetic analysis revealed rapid metabolism of NU7026 indicating that inhibition of repair could not be maintained (61). Screening of large libraries of NU7026 analogs lead to the identification of a number of compounds with increased selectivity for DNA-PK compared with other members of the PI3K family, as well as increased potency compared with previously generated compounds, including NU7441 (62). However DNA-PK inhibitors have not yet surpassed pre-clinical development. Despite a 2 fold increase in growth delay compared to DSB inducing agent etoposide alone, further development of compound NU7441 was abandoned due to limited aqueous solubility and oral bioavailability (63).

Other morpholine based inhibitors of DNA-PK have displayed both *in vitro* and *in vivo* radiosensitization in laboratory settings as well. Arylmorpholines, IC86621, IC87102 and IC87361 have been shown to increase the efficacy of radiation in tumour xenografts (64,65). Kashishian *et al.* (2003) showed *in vivo* efficacy of DNA-PK inhibitor IC86621 in xenografts in mice. Efficacy data was reported for a second morpholine derivative IC87361, in murine melanoma B16-F0 xenografts (64). Data shown indicates tumours treated with radiation alone were approximately 10 fold larger than tumours treated with radiation in combination with IC87361 when the study was concluded.

Inhibitors directed at other forms of repair, namely base excision repair, are also in development and are discussed in detail by Helleday *et al.* (2008) and will not be described here. If inhibition of repair could be made selective by exploiting a distinct feature of solid tumours, such as severe hypoxia, the efficacy of DNA damaging agents could increase while avoiding the systemic toxicity occurring from inhibition of repair in all tissues (55). Despite disappointing pre-clinical results for repair inhibitors thus far, advances in formulation and synthesis have given new hope to abandoned compounds. A nanoparticle formulation of wortmannin has been reported which has a maximum tolerated dose approximately five times greater than traditional formulations of the drug (66). Nanoparticle formulation improved solubility and stability resulting in lowered toxicity, indicating that this strategy may be applicable to other compounds which have failed due to problems with toxicity, solubility or unfavorable pharmacokinetics and pharmacodynamics.

## 1.6 Hypoxia activated prodrugs

Hypoxia activated prodrugs (HAPs) are inactive species which are converted by the body, spontaneously or metabolically, to the intended pharmacologically active component selectively under hypoxic conditions (67,68). Compounds of this class exploit the environment found within the hypoxic cell, namely enzymes which facilitate the reduction of these drugs from a non-toxic parent form to the active species in the absence of molecular oxygen (69,70). The severe difference in oxygen tension observed between tumours and normal tissues renders this an ideal approach to targeting therapy to solid tumours.

Typically prodrugs consist of three modular domains, a trigger, linker moiety and an effector unit, each optimized for specific function (67,71,72). The triggering molecule is key to hypoxia selectivity and must be a substrate for rapid bioreduction to a transient intermediate, that in the presence of molecular oxygen is back-oxidized to the prodrug form. For example, nitroaromatics which are reduced by endogenous cellular flavoprotein enzymes are considered convenient triggers. Figure 1.6 summarizes a typical mechanism for prodrug activation with a nitroaromatic trigger. The one electron adducts (nitro radical anion) which form from reduction can be scavenged by molecular oxygen thereby restricting activation to hypoxic cells. The effector is the pharmacologically active species, often previously established drugs which exhibit undesirable toxicity or solubility in normal tissue. Traditionally, the effector species have been very cytotoxic compounds, such as DNA-alkylating agents, which required prodrug forms to prevent systemic toxicity. While many newly developed prodrug candidates employ a cytotoxic

agent as an effector, some include chemical inhibitors with specific molecular targets (Minchinton et al. unpublished data)(71,73-75). The linker joins the effector and triggering components and functions to provide a high degree of deactivation of the effector while in the prodrug form and importantly, to efficiently release the effector upon reduction of the trigger molecule (71).

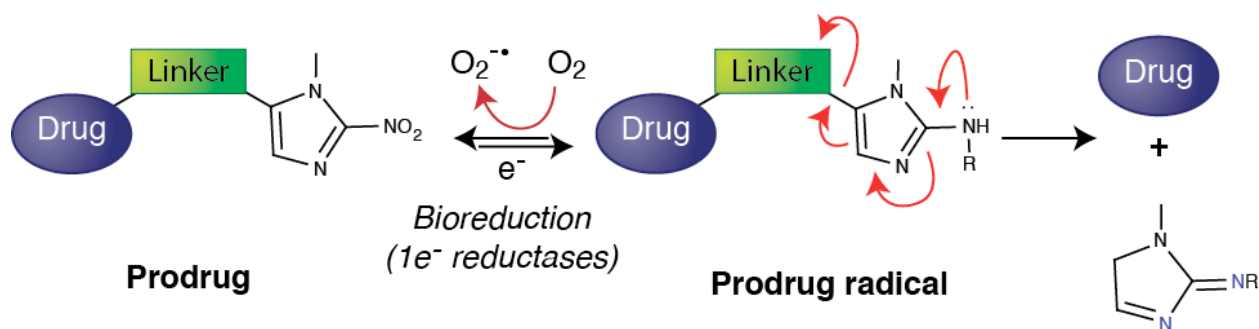


**Figure 1.6 Typical prodrug mechanism with nitroaromatic linker**

Typical mechanism for 2-nitroimidazol-5-ylmethyl prodrugs. The prodrug must be a substrate for intracellular 1e<sup>-</sup> reductases (15). Reductases, such as cytochrome P450 reductase, add an electron to the prodrug converting it to a prodrug radical. Under oxic conditions, the prodrug radical is rapidly back-oxidized to its non-toxic parent form, transferring the unpaired electron to molecular oxygen, forming a superoxide radical. Under hypoxic conditions, reduction of the nitro group to an amine prodrug radical (R = H or OH). The resulting pair of free electrons on the amino group triggers expulsion of the effector/drug moiety. Reprinted from Tetrahedron, Vol 59/19, Ferrer *et al.*, Studies on the reductively triggered release of heterocyclic and steroid drugs from 5-nitrothien-2-ylmethyl prodrugs, pp 3437-3444, Copyright (2003), with permission from Elsevier.

Combination of a hypoxia activated trigger with DNA repair inhibitors is the next logical step in the development of pharmaceuticals to increase the therapeutical benefit of conventional DNA damaging agents used in the therapy of solid tumours. Studies identifying and examining the metabolites of 2-nitroimidazoles highlight the use of the 2-nitroimidazol-5-yl methyl system as a triggering moiety to release amine-bearing drugs (56-58). TH-302, a 2-nitroimidazole prodrug of bromo-isophosphoramidate mustard,

significantly reduced the hypoxic fraction of several xenograft models in mice (76,77). Currently, phase 1 and 2 clinical trials are underway with promising results expected. PR-104, a water soluble phosphate ester, which is rapidly hydrolyzed *in vivo* to PR-104A, a dinitrobenzamide mustard was thought to undergo hypoxic specific reduction; however after entering clinical trials Guise et al. (2010) uncovered evidence of aerobic activation of PR-104A by an endogenous human aldoketoreductase, indicating limited hypoxic selectivity. These studies support the need for further development of HAPs and highlight the importance of metabolism by endogenous enzymes as a key factor when evaluating HAP compounds.

### **1.7 Formulation of insoluble drugs**

Poor aqueous solubility is increasingly a major hurdle in drug development (78,79). Advances in combinatorial chemistry and high throughput screening, as well as rational drug design has led to the development of new drugs with higher molecular weights and poor solubility (80-83). Several techniques have been developed by researchers in formulation science to alter the solubility and dissolution rate of compounds exhibiting poor solubility (68,83,84).

Surfactants have been shown to increase the solubility of many poorly water-soluble compounds through increasing particle wetting and interfering with crystal formation (63,85). Non-ionic polymeric surfactants coat the immiscible surface with hydrophobic chains, allowing for the projection of hydrophilic tails into aqueous solution, thereby increasing particle wetting (86). Repulsive steric forces between neighboring coated particles discourage crystallization and aggregation of (79).



Nano-sizing or milling is another technique to improve *in vitro* dissolution rate of poorly soluble compounds. Increasing the surface area can potentially yielding higher *in vivo* exposure. Nano-sizing reduces the active pharmaceutical ingredient particle size to the micron and submicron range and stabilizes particles with surfactants (79,87). While this technique has been in used in the pharmaceutical industry for several decades, advances in milling technology in recent years have permitted the production of particles on the order of 100 - 200 nm in size (88). Both 'bottom up' or 'top down' approaches are employed in the generation of nano-particles. 'Bottom up' mechanisms consist of building particles up from the molecular state, whereas 'top down' approaches rely on breaking larger micron-sized particles down, generally through milling (79,88,89).

## **Chapter 2: Materials and methods**

### **2.1 Inhibitor and prodrug**

1-{2-[(1-methyl-2-nitro-1H-imidazole-5-yl)methoxy]-4-(morpholin-4-yl)phenyl}ethan-1-one (Hapi3), M.W. 360.1 g/mol, was synthesized by Jason Tan at the Centre for Drug Research and Development (CDRD), Simon Fraser University. 1-(2-Hydroxy-4-morpholin-4-yl-phenyl)ethanone (IC86621) was synthesized in the laboratory of Gregory Drake, University of British Columbia Department of Chemistry according to previously published methods (90).

### **2.2 High pressure liquid chromatography**

Chromatographic analysis was performed on Waters HPLC equipment (Waters Limited, Mississauga, ON, CA), including a model 510 pump, a model 712 WISP injector, and a model 996 Photo-Diode Array (PDA) Detector. Sample separation was achieved with a Halo C18 column (4.6 x 50 mm, 2.7  $\mu$ mol/L). For separation of samples, a mobile phase consisting of a mixture of 36% (v/v) acetonitrile in ddH<sub>2</sub>O was used, at a flow rate of 1.5 mL/min. All eluents were prepared from HPLC grade products and degassed before running sample analysis by vacuum filtration. Hapi3 eluted after 1.5 min and IC86621 after 2.0 min. 5  $\mu$ L samples were injected and detection was carried out at  $\lambda$  = 320 nm and  $\lambda$  = 340 nm for Hapi3 and IC86621, respectively. Inhibitor and prodrug concentrations were determined from absorbance peak areas using an external standard curve.

### **2.3 Cell culture**

HCT116 human colorectal carcinoma cells were purchased from American Type Culture Collection (ATCC) and SCCVII murine squamous cell carcinoma cells were a gift from

James Evans. All cells were maintained in vented cap tissue culture flasks (Sarstedt Inc, 83.1810) with Minimal Essential Medium with Earle's Balanced Salts (MEM/EBSS, Thermo Scientific, Hyclone, SH30008.03) supplemented with 10% fetal bovine serum (FBS Qualified, Gibco, Invitrogen) referred to below as full MEM. Cells were passaged every 3 - 5 days upon reaching ~ 80% confluency. Standard incubation conditions for this thesis entail humidified incubator at 37 °C with 5% CO<sub>2</sub>, 5% O<sub>2</sub>, 90% N<sub>2</sub> atmosphere.

## **2.4 Resazurin assay**

Exponentially growing cells were harvested by enzymatic digestion with trypsin (Sigma-Aldrich Canada Ltd, T4049) and counted by haemocytometer. Cells were seeded in custom made 1.5 cm glass inserts for 24 well plates (BD Biosciences) at a density of 10<sup>4</sup> cells (HCT116 or SCCVII) per well in 500 µL media. Plates were incubated overnight for ~18 h under standard conditions. Following overnight incubation, media was aspirated from the inserts and replaced with 200 µL of full MEM containing either 0.15% DMSO or 50 µmol/L IC86621 and returned to incubator. Following 2 h drug incubation, plates were irradiated as described in section 2.6. Following irradiation, plates were returned to standard incubation conditions. Drug treatments remained on the cells for 22 h following radiation (24 h total) after which drug-containing media was aspirated off and replaced with 500 µL of full MEM. Cells were allowed to incubate for an additional 48 h. Following incubation, 2.2 mmol/L resazurin prepared in full MEM was added to a final concentration of 315 µmol/L. Resorufin (a resazurin reduction product) fluorescence was measured hourly following addition of resazurin using a TECAN GENios plate reader (excitation  $\lambda$  = 535 nm: emission  $\lambda$  = 590 nm), gain 60, 40 µs

integration with 5 flashes per well. A score for percent cell viability was generated by subtracting the background fluorescence of blank wells (media + resazurin) and normalizing to the unirradiated vehicle controls. Mean percent cell viability for two independent experiments, each with  $n = 6$  replicates per treatment group, was plotted against radiation dose using Prism 5.0d (GraphPad Inc.) to compare drug relative to vehicle treated cells.

## **2.5 Radiation treatment**

Cells were irradiated in custom built aluminum chambers constructed by Andrew I. Minchinton and Alastair H. Kyle, containing a multi-attenuating insert, also designed by Kyle. The multi-attenuator was designed such that two 24 well plates fit within the aluminum chambers and a gradient of attenuating materials (brass and lead) produces six defined radiation doses across the six columns of a 24-well plate. Thermoluminescent dosimetry was performed to determine the percent attenuation for each column of the 24-well plate. For local tumour irradiation, mice were secured into custom built jigs consisting of plexiglass housing 30 mm x 30 mm x 70 mm (H x W x L), with movable front piece to adjust for body length of the mouse. A lead layer 2 mm thick covered the lower portion of the jig to attenuate radiation, protecting normal tissue. Dosimetry was performed with a Victoreen radiation dosimeter. Mice were secured in jigs with tape. Radiation dose was split between two doses, such that each side of the tumour received half the total dose.

## **2.6 Prodrug formulation**

Hapi3 formulations were prepared by Matthew Wong or Carlos Fleet in the laboratory of Dr. Norbert Maurer, CDRD, University of British Columbia. A stock solution was

prepared by dissolving Hapi3 in 0.2% Solutol® HS-15 in DMSO and heated at 85 °C for 1 h until completely dissolved for a final concentration of 50 mg/mL. The stock solution was added to rapidly stirred 0.2% Solutol® HS-15/0.9% NaCl to a final concentration of 0.5 mg/mL Hapi3. The resulting crystalline suspension was split into 15 mL tubes and centrifuged at 2885 x *g* for 120 min at 4 °C with deceleration set to 1 (slow). Tubes were decanted to remove any significant traces of DMSO. DMSO is removed such that the resulting formulation was a homogenous suspension of Hapi3. Homogeneity is an important parameter to ensure consistent drug delivery. Pellets were combined and distributed equally among four tubes. Pellets were resuspended in cold 0.5% Solutol® HS-15/0.9% NaCl and the above centrifugation and decant procedure repeated. Resulting pellets were combined into two glass vials. An equal volume of yttrium-stabilized zirconium oxide beads (Ceroglass, ZYP-96015) was added to each vial and stirred at the maximum setting with magnetic stir bars for 18 h. The contents of each vial were transferred to a 70 µm cell strainers (BD Falcon, 352350) and filtered by centrifugation at 1000 x *g* for 2 min. Beads and vials were rinsed with 0.5% Solutol® HS-15/0.9% NaCl, centrifuged in the cell strainer as above and repeated for a total of 4 washes. The resulting suspensions were combined and administered to mice the following day. Stability of formulations was assessed by measuring crystal particle size by light microscopy. Chemically stability following formulation was assessed by HPLC. Particle size measurements were obtained upon receipt of formulations, as well as before administration to mice and weekly for up to four weeks following the initial date.

## **2.7 Blood and tissue sample collection and processing**

Blood samples were collected by saphenous or tail vein puncture in accordance with the UBC Animal Care Committee Policy on Acceptable Methods of Rodent Blood Withdrawal. Blood was collected with heparinized microcapillary tubes and stored on ice until processing. In microcentrifuge tubes, blood and an equal volume of 6%  $\text{ZnSO}_4 \cdot 7 \text{H}_2\text{O}/\text{MeOH}$  were vortexed for 30 sec to deprotonate and extract the prodrug from tissue homogenate. Samples were centrifuged at  $21\,000 \times g$  for 10 min. Tissue samples including hind leg muscle, kidney, lung, heart, liver, spleen and brain were excised following cardiac puncture. Samples were placed in individual Petri dishes on ice, rinsed with saline, blotted dry and placed in sample collection tubes. Subsequently, tubes were weighed and frozen in liquid nitrogen. All samples were stored at  $-20\text{ }^\circ\text{C}$  and processed the following day. Frozen tissue samples were thawed on ice. Tissue and three volumes of sterile ice cold ultra pure water were placed in a glass dounce paired with a well fitted teflon pestle. Tissues were homogenized by hand for 1 - 2 min or until tissue appeared homogenous and free of large chunks. Equal volumes of homogenate and 6%  $\text{ZnSO}_4 \cdot 7 \text{H}_2\text{O}/\text{MeOH}$  were pipetted into microcentrifuge tubes and vortexed for 30 sec. Samples were centrifuged at  $21\,000 \times g$  for 15 min. Supernatant was removed and analyzed by HPLC.

## **2.8 *In vivo* efficacy studies**

Male and female Rag2M mice were purchased from Charles River Laboratories International, Inc. Female NOD/SCID mice were bred in our institutional animal facility. All mice were maintained in our animal facility in accordance with the Canadian Council on Animal Care guidelines.  $10^7$  HCT116 or  $10^6$  SCCVII cells in  $50\text{ }\mu\text{L}$  MEM media was

subcutaneously implanted into the sacral region of male Rag2M mice, aged 7 - 9 weeks. Tumours were measured using calipers and volume was calculated using three orthogonal diameters (a, b and c) using the formula  $\text{volume} = \pi/6(abc)$ . For efficacy studies, once tumours reached 150 - 200 mm<sup>3</sup> in volume, mice were treated with 1600  $\mu\text{mol/kg}$  Hapi3 or equivalent volume of vehicle control (0.5% Solutol® HS-15/0.9% NaCl) by oral gavage. 3 h post gavage, tumours were locally irradiated, receiving 0 Gy or 15 Gy. Tumours were measured as described above five days per week for three weeks and three times per week until tumours reached 1000 mm<sup>3</sup>. The experiments described in this thesis were approved by the Animal Care Committee of the University of British Columbia. All mice were permitted access to standard laboratory rodent food and water.

## **2.9 Statistical analysis**

Mean and standard deviation (SD) or standard error of the mean (SEM) were calculated for each variable studied when sufficient replicate number allowed. GraphPad PRISM software was used to conduct an unpaired two-tail t-test to assess significance of differences in cell viability between treatment groups in section 5.1. GraphPad PRISM was also used to conduct a one-way ANOVA analysis when appropriate to compare changes in tumour volume such as in section 5.3.

## Chapter 3: High pressure liquid chromatography assay to quantitate Hapi3

### 3.1 Assay validation

#### Introduction

We developed a simple and rapid HPLC procedure for quantification of Hapi3 in solution. To determine the potential limitations of this assay, linearity and the limits of detection and quantitation were determined.

#### Approach

Standard solutions of Hapi3 ( $n = 3$ ) were prepared in 6% zinc sulphate in methanol ranging in concentration between 0.1 - 150.0 (0.1, 6.3, 12.5, 25.0, 50.0, 100.0 and 150.0  $\mu\text{mol/L}$  and analyzed by HPLC as described in methods and materials section 2.2. The presence of zinc sulphate was to aid in protein precipitation in tissue homogenate samples in later experiments. Linearity of the calibration curve was determined through regression analysis by evaluating the slope and determination coefficient ( $R^2$ ) of a Hapi3 standard curve. Regression equation were calculated according to the formula  $y = mx + b$ , where  $y$  is the AUC obtained from integrating Hapi3 chromatograms,  $m$  is the slope,  $x$  is the concentration of Hapi3 ( $\mu\text{mol/L}$ ) and  $b$  is the  $y$  intercept. The limit of detection was expressed as  $\text{LOD} = 3.3\sigma/S$ , where  $\sigma$  is the standard deviation of the response and  $S$  is the slope of the calibration curve.  $\sigma$  was determined based on the calibration curves using the standard deviation of  $y$ -intercepts of regression lines in accordance with the ICH Harmonized Tripartite Guidelines. The limit of quantitation was expressed as  $\text{LOQ} = 10\sigma/S$ ,  $\sigma$  and  $S$  defined as above.



## Results and Discussion

A calibration curve consisting of external standards was obtained for Hapi3 by comparing the area under the curve (AUC) against respective known concentrations. Regression analysis resulted in an  $R^2$  value of  $> 0.99$ , as shown in Figure 3.1, indicating extremely good fit. Slope, intercept and determination coefficient of regression equations resulting from Hapi3 calibration curves are summarized in Table 3.1. Using the HPLC method specified in section 2.2, the LOD was estimated to be  $0.4 \mu\text{mol/L}$ , whereas the LOQ was estimated to be  $1.2 \mu\text{mol/L}$ .

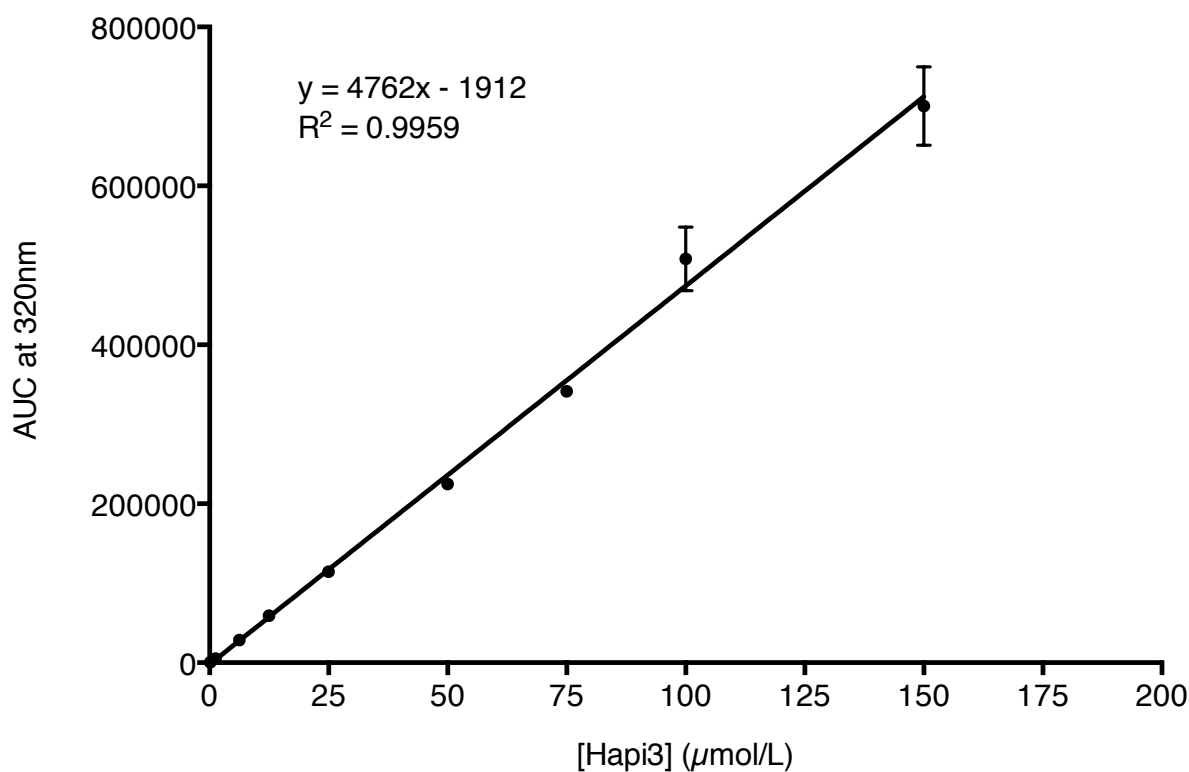


**Figure 3.1 Hapi3 calibration curve constructed with external standards of Hapi3 in methanol/6% ZnSO<sub>4</sub>.**

$r^2$  values are  $\geq 0.99$ ,  $n = 5$ . a.u.c, area under the curve for Hapi3 peak eluting from the HPLC. Bars, standard deviation of the means.

**Table 3.1 Slope, intercept and determination coefficient of regression equations resulting from Hapi3 calibration curves**

Run	Slope	Intercept	R <sup>2</sup>
1	4173.1	5804.2	0.9974
2	4876.1	2970.4	0.9976
3	4885.3	4167.1	0.9951
4	4919.5	3858.3	0.9943
5	4954.9	4368.1	0.9949
Average*	4761.8 ± 148	4233.6 ± 460	0.9959 ± 0.0007

\*Mean ± SEM

### 3.2 Sample matrix effects and recovery from tissue

#### Introduction

To determine the optimal time for IR therapy *in vivo*, pharmacokinetic information regarding peak concentration in tissues and plasma was needed. *In vivo* tissue concentrations depend not only on the effective diffusion of Hapi3 through the extracellular space but uptake and metabolism by cells, movement across membranes, structure of vasculature within the tissue and blood flow. Before starting basic plasma and tissue studies to examine Hapi3 levels following administration, it was necessary to examine the effects of various tissue matrices on the detection and quantification of Hapi3. Interference from the sample matrix may compromise the reliability and selectivity of the assay, leading to false positive results (91). Similarly, to accurately determine tissue concentrations extraction efficiency or percent recovery of Hapi3 was determined.

#### Approach

To assess Hapi3 extraction efficiency, plasma and tissue homogenate samples from untreated animals were spiked with stock solutions of Hapi3 prepared in DMSO to a

final concentration of 1.3, 2.5, 5.0, 10.0 and 20.0  $\mu\text{mol/L}$  ( $n = 3$ , for each concentration) to generate tissue calibration curves were prepared.

Precipitation of protein and extraction of Hapi3 was achieved by the addition of 60%  $\text{ZnSO}_4$  (volume equal to 10% of sample volume) and methanol (volume equal to 90% of sample volume) and vortexed for 30 sec. Protein and debris was pelleted by centrifugation at  $15\,000 \times g$  for 15 min. Subsequently supernatant was removed and placed in glass HPLC vials for analysis as described in section 2.2. Recovery of Hapi3 from tissue is expressed as  $(\text{AUC for spiked homogenate}/\text{AUC in methanol}) \times 100$ .

## **Results and Discussion**

Extraction efficiency for Hapi3 from murine plasma and tissue homogenate at 5.0, 10.0 and 20.0  $\mu\text{mol/L}$  was determined. The extraction efficiency from various tissues is summarized in Table 3.2 as mean percent yield  $\pm$  SEM. Extraction efficiency varied between tissues, ranging from  $98.9 \pm 2.3 \%$  in muscle to  $> 100\%$  in most other tissues. The mean extraction efficiency from plasma was  $102.4 \pm 2.8 \%$ . Tissue calibration curves are summarized in Figure 3.2. All curves exhibited determination coefficients ( $R^2$ )  $> 0.99$  indicating good linear fit. Several tissues yielded recovery values greater than 100%. The recovery values presented in Table 3.2 imply the assay overestimates Hapi3 levels in tissue homogenate, ranging from  $\sim 2 - 16 \%$ .

The assay designed to quantitate Hapi3 in various murine tissues over estimated total Hapi3, as is indicated by the average tissue recovery of  $105 \pm 3 \%$ . The overestimation in yield may have resulted from several factors. Pipetting of volatile liquids such as methanol must be performed rapidly to prevent evaporation and dripping of the liquid

from the tip. Tips were pre-rinsed with methanol to improve accuracy, as recommended by the pipette manufacturing guidelines, however errors in pipetting may have contributed to the observed error. It is unlikely the error resulted from incorrect dilution of the Hapi3 stock solution, as the concentration of solutions prepared for spiking tissue homogenate were confirmed by HPLC before use. The total volume of the extract must be measured for calculation of the final concentration, any inaccuracy would greatly impact the error.

Interference from the sample matrix can greatly affect detectability and quantification close to detection limits (92). No signal was observed at  $\lambda = 320$  nm in samples of homogenate spiked with vehicle (DMSO), therefore it is unlikely that the overestimation resulted from tissue matrix effects. These samples were analyzed following spiked samples of homogenate of the same type to ensure no Hapi3 remained bound to the column, contaminating subsequent runs. The principle function of the assay was to reliably estimate plasma and tissue concentrations such that various formulations could be tested as this information was required to determine the most suitable time point to deliver radiation following administration of the prodrug. Chromatography combined with mass spectroscopy as oppose to absorbance detection may yield more sensitive quantitation, however for our purposes the degree of error was acceptable. Similarly, if a radiolabelled atom such as tritium ( $^3\text{H}$ ) could be incorporated into the inhibitor portion of the prodrug, Hapi3 levels could be determined more definitively.

**Table 3.2 Average extraction efficiency of Hapi3 in plasma and tissues.**

Spiked tissue homogenate was prepared from a standard solution of Hapi3 in DMSO and drug-free homogenates of tissues to maintain matrix consistency between the standards and tissue homogenates. See Appendix B for a more detailed explanation and sample calculation.

Plasma (%)	Muscle (%)	Lung (%)	Liver (%)	Kidney (%)	Brain (%)	Tumour
102.4 ± 2.8	98.9 ± 2.3	116.4 ± 0.31	102.6 ± 8.2	102.7 ± 0.1	109.6 ± 3.2	101.4 ± 3.0

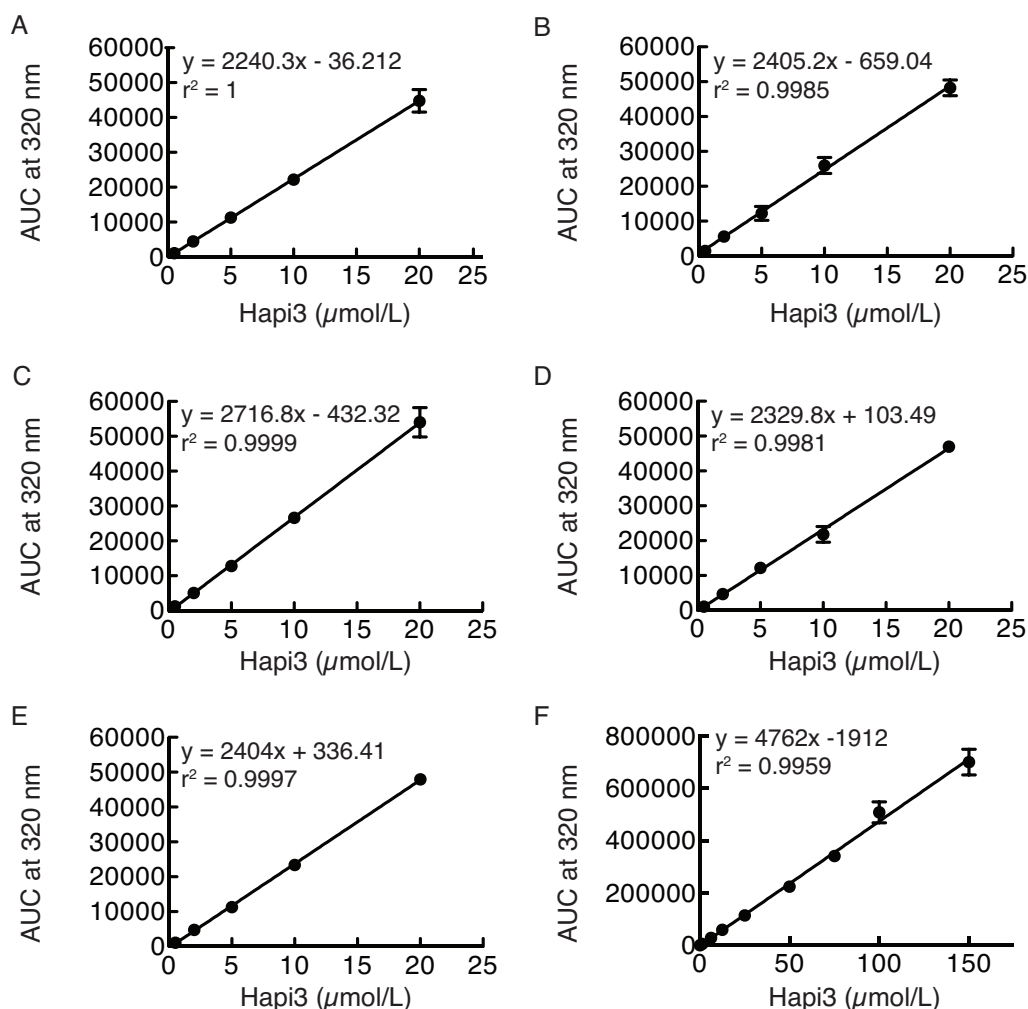


**Figure 3.2 Tissue calibration curves constructed using HPLC analysis of Hapi3 added to tissue homogenates.**

Curves A - E plot area under the curve (AUC) for tissue homogenate extracts against concentration of Hapi3 in spiked tissues; A) muscle, B) brain, C) lung, D) liver, E) kidney F) Hapi3 in 6% ZnSO<sub>4</sub>/MeOH.  $r^2$  values are  $\geq 0.99$ ,  $n = 3$ . Bars, standard deviation of the mean. A.U.C. An equal volume of MeOH/6% ZnSO<sub>4</sub> was used to extract Hapi3 from tissue homogenate, introducing dilution of the sample by a factor of 2, accounting for the difference in slopes observed in A - E relative to F. See Appendix B for a more detailed explanation and percent recovery sample calculation.

## Chapter 4: Hapi3 formulation for *in vivo* studies

### 4.1 Formulation of Hapi3 with block copolymers and milling

#### Introduction

Poor aqueous solubility of Hapi3 presented considerable challenges when developing formulations for pharmacological and efficacy assessment. Poor solubility is a significant hurdle in developing formulations for *in vivo* administration that will achieve adequate bioavailability. Solubility as well as permeability are considered the main factors contributing to bioavailability (69,93). A sensitization enhancement ratio of 1.8 (SF 0.001) was achieved *in vitro* with 100  $\mu\text{mol/L}$  Hapi3 in media in when applied to cells gassed at 0.1%  $\text{O}_2$  (Minchinton et al. unpublished data). Accordingly, 100  $\mu\text{mol/L}$  was chosen as the desired *in vivo* concentration which would achieve radiosensitization. We achieved Hapi3 formulations of 3.6 mg/mL in 10% DMSO/60% PEG-400 in 30 mmol/L sodium acetate buffer pH 4.5 and 10% DMSO/40% EtOH in 10 mmol/L sodium acetate buffer pH 4.5 however more concentrated formulas were necessary to achieve the desired dose of 100  $\mu\text{mol/L}$  in systemic circulation. To achieve more concentrated formulations with the aim of achieving adequate bioavailability we obtained assistance from the Drug Delivery Division at the Centre for Drug Research (CDRD), Vancouver. Discussion with formulation chemists at CDRD ultimately determined that Hapi3 would likely exhibit poor solubility in a wide variety of commonly used formulation solvent and that employing surfactants and cosolvents and a more favorable approach would be to try to stabilize crystal size and structure in the sub-micron range. My role in these efforts was to examine size and stability of Hapi3 crystals in formulations prepared by Matthew Wong and Carlos Fleet in Dr. Norbert Maurers laboratory at the CDRD. Also, I was

responsible for conducting small ( $n = 1 - 2$ ) tolerability studies, in which limited pharmacokinetic assessment was also performed. An increase in surface area from reduction of particle size is reported as a widely used, simple and effective method to increase dissolution rate of poorly water-soluble compounds (94). Both parties came to the conclusion that a further reduction in particle size, preferably a suspension of crystals on the nanometer scale, might yield a more concentrated formulation, allowing for increased dose to animals and possibly increased absorption as well owing to the increase in particle surface area.

### **Approach**

To develop a more concentrated formulation than possible due to the limited aqueous solubility of Hapi3, crystalline solid dispersions of Hapi3 and ball-milling was assessed with the aim of reducing particle size. To generate crystals with homogenous size and shape, a super saturated solution of Hapi3 was generated by dissolving Hapi3 in DMSO or tetrahydrofuran (THF) under heat and subsequently adding the resultant mixture drop-wise to solutions of surfactants in saline (Solutol® HS-15) while mixing with a hand held homogenizer or THF (P8677-SEO and P9083-SEO). In this manner fine, ordered crystals were generated and stabilized by the added surfactant. For Solutol® formulations, resulting crystalline suspensions were separated into tubes and centrifuged to concentrate crystals in solution and remove DMSO. Pellets were resuspended in cold 0.5% Solutol® in saline and stored overnight. Centrifugation and solvent removal was repeated. For THF-surfactant Hapi3 solutions, saline was added drop wise. Water and THF were removed under vacuum and the product was freeze-dried.

As formulation development continued, an approach to further reduce crystal size in Solutol® formulations was employed. Wet-milling with zirconium silicate beads was used to physically disrupt crystals and reduce crystal size. Beads were allowed to mill the concentrated crystalline suspension for 18 h at room temperature. Conventional or polarized light microscopy was used to image and measure crystal size.

## **Results and Discussion**

Initial formulations consisting of 0.2% (w/v) Solutol® contained crystals ranging 20 - 50  $\mu\text{m}$  in length, shown in Figure 4.2 A. Increasing the concentration of Solutol® to 0.5% appeared to stabilize smaller crystals in solution and prevent aggregation (Figure 4.2 B). However, the maximal concentration of Hapi3 in solution under these conditions was  $\sim 10 \text{ mg/mL}$ . To increase solubility and concentration of Hapi3 in solution additional surfactants, as well as milling techniques were employed to generate formulations with improved bioavailability. Formulations consisting of block copolymers of polystyrene and ethylene oxide were generated, shown in Figure 4.3; however no toxicity information was available for these compounds. Formulations were prepared such that the ratio of Hapi3/polymer was 5%. Both polymers produced unacceptable signs of toxicity and were not developed further. Methods to increase dissolution are also known to increase bioavailability as well. A wet-milling approach was used to reduce particle size further, with the aim of increasing solubility as well as increasing bioavailability. Wet-milling with zirconium silicate beads reduced particle size to  $\leq 5 \mu\text{m}$ , shown diluted suspension in Figures 4.4 A and 4.4 C. However, microscopy of the undiluted milled suspension (Figure 4.4 B) showed that the micron sized particles aggregated into larger clusters. Ball-milling produced a formulation with a final Hapi3 concentration of 28 mg/mL.



Hapi3 presented considerable formulation challenges for *in vivo* work. Hapi3 exhibits very poor solubility in aqueous solutions, < 1 mg/mL. First attempts at formulating Hapi3 used surfactants to increase solubility. Surfactants have been shown to improve particle wetting and dissolution, decrease or prevent drug precipitation and degradation, assist in drug uptake and modification of release (63). Initial solubility testing by the CDRD determined that acid titration and excipients such PEG400 and propylene glycol (40 - 60%) and mixtures of the two, failed to improve the solubility of Hapi3. Crystalization of Hapi3 occurred within minutes - hours upon mixing. 3 - 3.6 mg/mL was determined to be the maximum solubility in 10% DMSO/60% acidified PEG400. For initial tolerability and toxicity testing a more concentrated solution was desired, in excess of 10 mg/mL.

Suspension formulations are often used in animal studies involving poorly soluble compounds and was determined to be the most suitable course of action for Hapi3 (59). Initial tolerability testing employing i.p. administration determined the maximum tolerated dose to be ~ 600  $\mu$ mol/kg, yielding a Cmax in plasma of 30 min with a half life of about 1 h. However, oral administration was better tolerated at this dose, with no observable side effects or apparent toxicity and was used for subsequent experiments.

Improvements in bioavailability and dosing were achieved by increasing particle surface area. Ball-milling reduced the average particle size 5 - 10 fold, producing crystals ~ 5  $\mu$ m in diameter. Crystal size remained stable for > 2 weeks, with only slight increase in size and aggregation of crystals at 4 weeks. Formulation development and testing used ~ 40 - 50 % of the available raw Hapi3 material. As such, limited pharmacokinetics were examined during tolerability studies and are discussed below.

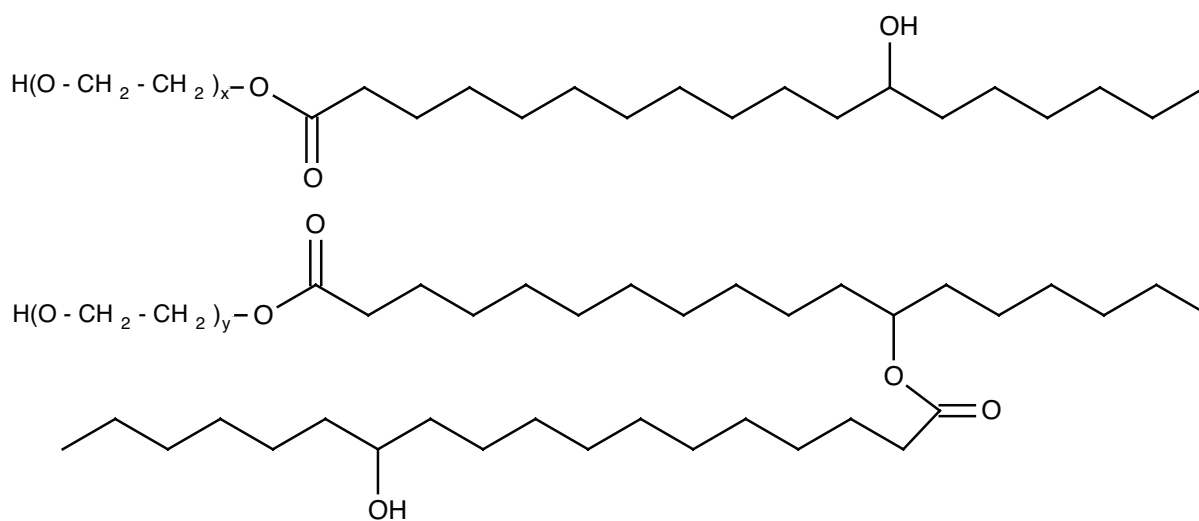


**Figure 4.1 Solutol® HS-15 structure.**

Shown are the main components of the lipophilic component of Solutol® HS-15, which consists of polyglycol mono- (top) and di-esters (bottom) of 12-hydroxystearic acid.

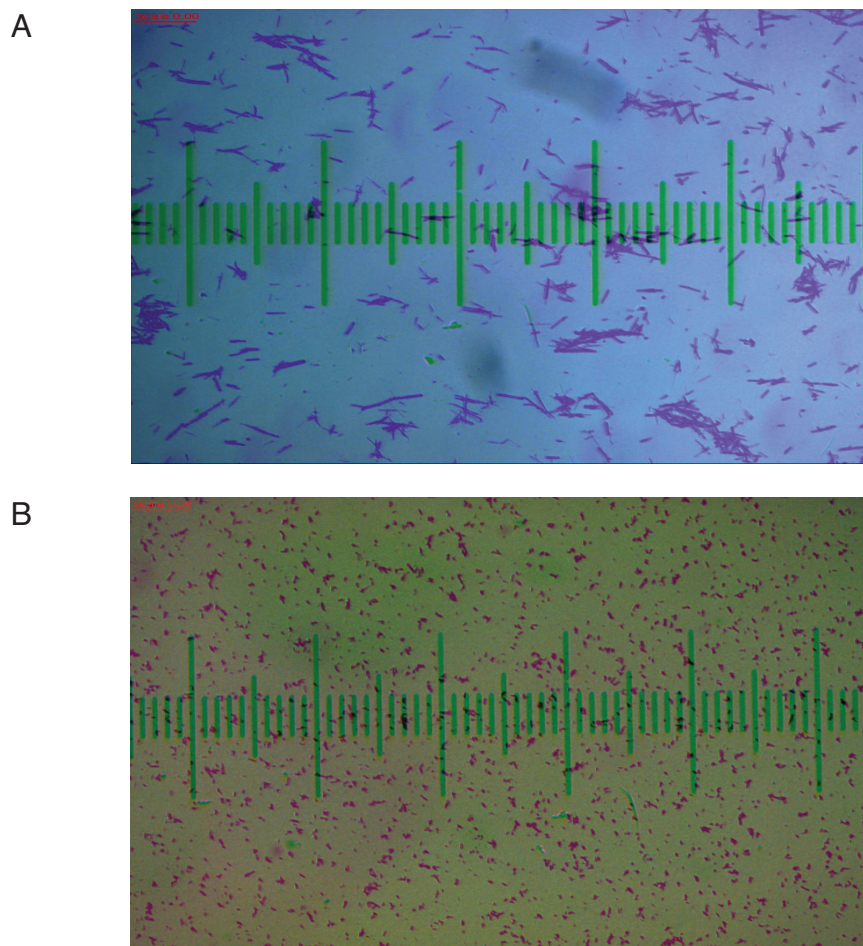


**Figure 4.2 Brightfield microscopy of Hapi3 crystalline suspensions.**

A) Polarized microscopy of 11.4 mg/mL Hapi3 suspension. B) 10.1 mg/mL suspension of Hapi3. Suspension diluted 20 fold. 1 division, 10  $\mu\text{m}$ .

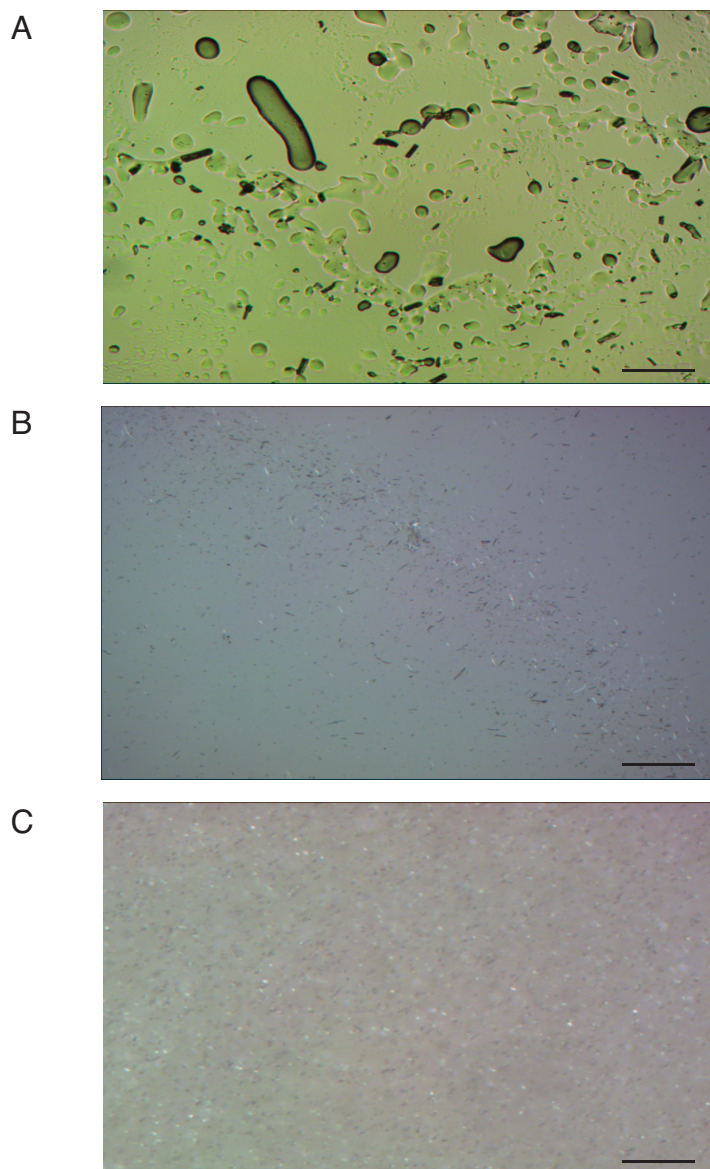


**Figure 4.3 Brightfield microscopy of Hapi3 crystalline polymer suspensions.**

A) Poly(styrene-b-ethylene oxide) diblock copolymer P8677-SEO. B) Poly(styrene-b-ethylene oxide) diblock copolymer P9083-SEO. C) Magnetic stir bar milled Solutol® HS-15 diblock copolymer suspension. Suspensions diluted 20 fold. Scale bar, 50  $\mu\text{m}$ .

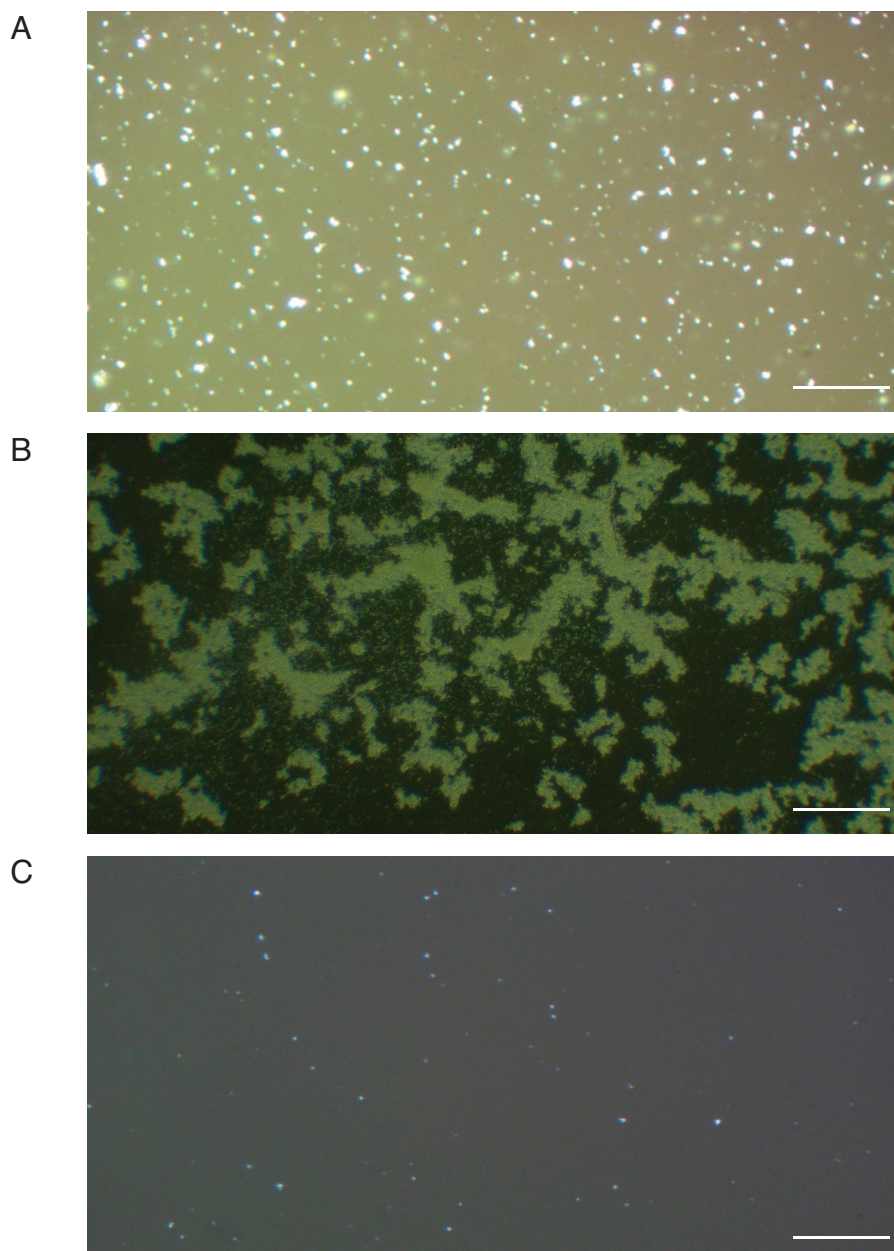


**Figure 4.4 Brightfield microscopy of ball-milled Hapi3 crystalline suspensions.**

A) Polarized microscopy of 15 mg/mL Hapi3 suspension, diluted 100 fold. Scale bar,  $100\mu\text{m}$ . B) conventional microscopy of 28 mg/mL suspension of Hapi3, undiluted. Scale bar,  $200\mu\text{m}$ . C) Suspension indicated in B), diluted 500 fold. Scale bar,  $100\mu\text{m}$ .

## Chapter 5: Biodistribution and efficacy testing

### 5.1 DNA-PK inhibition sensitizes H460 and SCCVII cells to ionizing radiation *in vitro*

#### Introduction

Previously, our lab has shown *in vitro* Hapi3 efficacy in HeLa cervical carcinoma and H460 non-small cell lung carcinoma cell lines. For *in vivo* testing, we wished to examine two tumour xenograft models which display predominately different forms of hypoxia. HCT116 human colorectal carcinoma cells were chosen as this model displays more acute or perfusion limited hypoxia and SCCVII murine squamous cell carcinoma cells were chosen for their higher prevalence of chronic or diffusion limited hypoxia. The resazurin reduction assay was used to examine Hapi3 efficacy in these cell lines.

The resazurin reduction assay is a simple and efficient way to non-destructively measure the response of cells to radiation. Traditionally colony forming assays are used to score radiation response, however survival assays require a large number of plates, sufficient time for colony formation, often 10 - 14 days and scoring by an individual. The resazurin reduction assay is an attractive alternative. The assay measures the ability of viable cells to enzymatically reduce the resazurin sodium salt to hydroresorufin (95,96). The reduction scheme for resazurin is shown in Figure 5.1. Resazurin is also commonly referred to commercially as Alamar Blue. Compared with the time required for colony forming assays, the resazurin assay is more rapid, requiring only a few hours. Reduction of resazurin to resorufin and eventually dihydroresorufin occurs only in viable, metabolically competent cells (95). Therefore, the production of resorufin serves as a means to measure the effects of cytotoxic injury. The effects of DNA-PK inhibition



on HCT116 and SCCVII were examined in concert with radiation by the resazurin reduction assay to determine if these cells would be appropriate for efficacy testing of Hapi3 in mice.

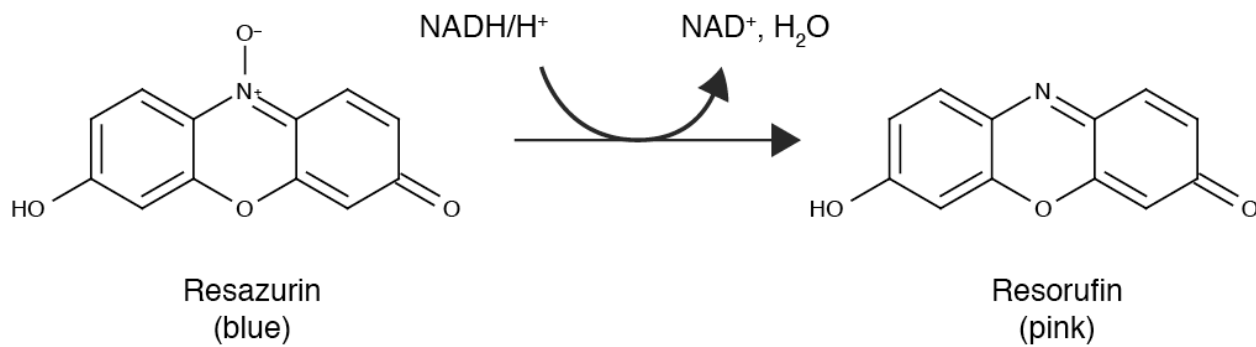


### Figure 5.1 Reduction of resazurin to resorufin

Oxidized, non-fluorescent resazurin is reduced by cellular reductases to fluorescent pink resorufin by mitochondrial, microsomal and cytosolic oxidoreductases (97).

### Approach

In this experiment Hapi3 was added to both SCCVII and HCT116 cells at 50  $\mu\text{mol/L}$  in media and incubated for 2 h under standard conditions in glass tissue inserts in 24 well plates. The control group was treated with 0.15% DMSO, such that equal concentrations of the vehicle were present in the control and Hapi3 treatment groups. Following incubation, plates were removed from incubators and irradiated in our aluminum chambers containing the multi-attenuator insert described in materials and methods section 2.6, receiving doses ranging from 0.3 - 5 Gy. Following IR, plates were returned to standard incubation conditions for 22 h. Subsequently, media containing drug was removed and replaced with 500  $\mu\text{L}$  fresh MEM and returned to standard incubation conditions for an additional 48 h. This allows the cells to recover following radiation and allows for sufficient time for the effects of the treatment to be observable.

Following this recovery period, cells were incubated with 315  $\mu\text{mol/L}$  resazurin in standard media under standard conditions for 5 hrs. Resorufin fluorescence was read by plate reader (excitation  $\lambda$  535 nm: emission  $\lambda$  590 nm) as described in the materials and methods, section 2.4. Cell viability was determined by normalizing resorufin fluorescence readings such that the blank fluorescence was defined as 0% and the mean fluorescence of DMSO unirradiated controls was defined as 100%.

## Results and Discussion

Figures 5.2 and 5.3 display cell viability data for HCT116 and SCCVII cells respectively, treated with 0 - 5 Gy IR in combination with 50  $\mu\text{mol/L}$  IC86621 or 0.15% DMSO (vehicle control). DNA-PK inhibition by IC86621 provides radiosensitization at IR doses between 1.2 - 3.8 Gy as indicated by significantly lower viability relative to vehicle treated cells at the same dose of IR ( $p < 0.01$ ). All SCCVII cells treated with IC86621 exhibit lower cell viability following radiation, indicating reduced cell survival relative to controls.

While our group has produced clonogenic survival data for Hapi3 in combination with radiation in HeLa and H460 cell lines as well as resazurin cell viability data with DNA-PK inhibitor IC86621 in murine CB.17 and H460 cells (Minchinton *et al.*, unpublished data), there was no data regarding repair inhibition in murine SCCVII and human HCT116 cell lines. Inhibition of DNA-PK in combination with DSB induction by IR resulted in decreased cell viability as measured by resazurin reduction in both models (Figures 5.2 and 5.3). Interestingly DNA-PK inhibition alone reduced cell viability in SCCVII cells (Figure 5.3, 0 Gy). Reduction in viability was not observed in human H460 or HCT116 cell lines and may be explained by the observation that murine cell lines



display up to approximately 50 - 100 fold less DNA-PK than human cells, as measured by activity and expression (98,99). Exponentially growing SCCVII cells double at twice the rate (~ 15 h) relative to HCT116 and H460 cells (25 and 20 h, respectively). Future studies should account for these differences by performing the assay for the slower growing lines 10 - 15 h following the SCCVII cells. Inhibition of DNA-PK may not only decrease or inhibit NHEJ but affect HR as well, resulting in irreparable DSBs generated from stalled replication forks or normal metabolism. While the greatest statistically significant differences were seen between cells dosed with 1.2 - 3.8 Gy, the similarity in viability between treatment groups at 5 Gy likely results from lack of sensitivity of the assay at low cell densities. The clonogenic survival assay is more sensitive, however in appropriate for HCT116 cells as they form doublets or triplets upon enzymatic digestion. Both HCT116 and SCCVII cells exhibited sensitization to radiation following DNA-PK inhibition, which supported these models as appropriate for *in vivo* evaluation.

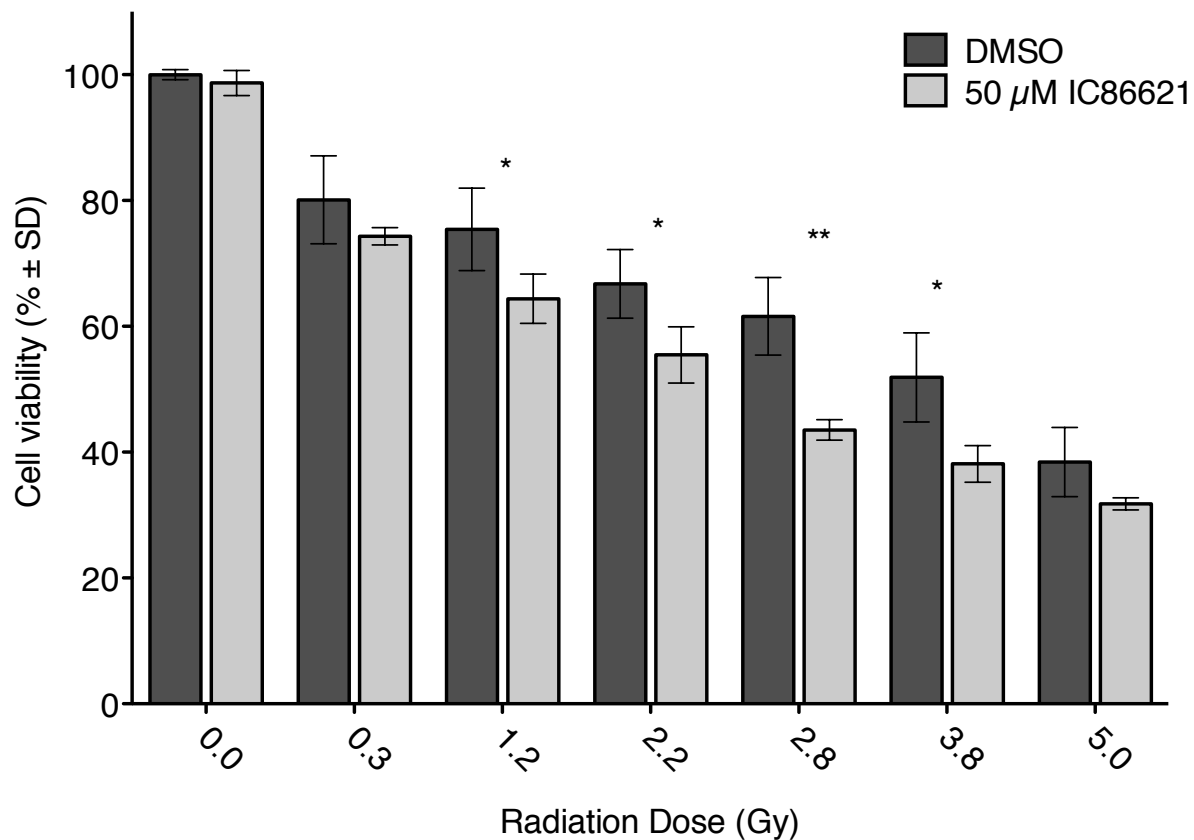


**Figure 5.2 Effects of DNA-PK inhibition by IC86621 in combination with radiation in HCT116 cells.**

The resazurin reduction assay was used to examine cell viability in HCT116 cells following treatment with 50  $\mu\text{mol/L}$  IC86621 in combination with radiation. Percent cell viability  $\pm$  SD was plotted against radiation dose (Gy). A t-test was conducted to evaluate differences in percent viability between treatment groups for each dose. (\*  $0.01 < p < 0.05$ ; \*\*  $0.001 < p < 0.01$ ).

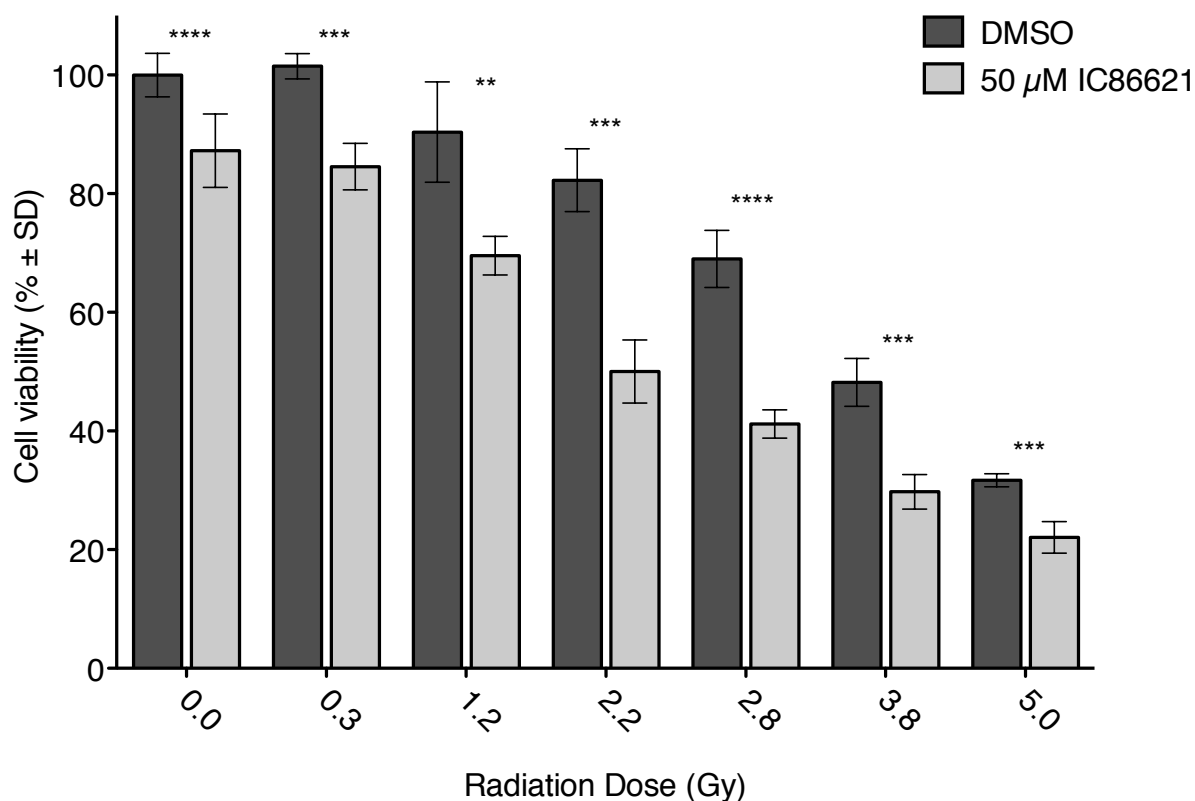


**Figure 5.3 Effects of DNA-PK inhibition by IC86621 in combination with radiation in murine SCCVII cells.**

The resazurin reduction assay was used to examine cell viability in SCCVII cells following treatment with 50  $\mu\text{mol/L}$  IC86621 in combination with radiation. Percent cell viability  $\pm$  SD was plotted against radiation dose (Gy). A t-test was conducted to evaluate differences in percent viability between treatment groups for each dose. \* $p = 0.01 - 0.05$ ; \*\* $p = 0.001 - 0.01$ ; \*\*\* $p < 0.001$ ; \*\*\*\* $p < 0.0001$ .

## 5.2 Concentration of Hapi3 in blood plasma and biodistribution studies

### Introduction

The crystalline ball-milled microsuspension of Hapi3 was determined to be the most suitable formulation for efficacy testing. Attempts to improve Hapi3 solubility through the addition of polar functional groups were unsuccessful. Appreciable time may be required in order for the prodrug to diffuse from the vasculature within the tumour to the distant hypoxic cells (33). Studies examining the repair kinetics of DSBs following radiation by evaluation of  $\gamma\text{H}_2\text{AX}$  foci have shown that DSB repair has both a fast as well as a slow component. However, a majority of repair occurs in the first 4 h following irradiation (100,101). The inhibitor must be present at sufficient concentrations to inhibit repair at the time of radiation and ideally in the hours that follow while the slow component of repair occurs (61). Kinetic studies comparing the rate of repair in murine scid and corresponding parental CB.17 cells determined that scid cells, which harbor a mutant form of DNA-PK, require 4 - 6 h to repair a majority of damage induced by IR compared with 1 h in CB.17 cells (102). To determine if the required prodrug levels to produce radiosensitization could be achieved *in vivo*, tolerability and quantification of the prodrug were conducted examining both plasma and tissue concentrations of the prodrug.

### Approach

Mice were administered either 580, 750 or 1600  $\mu\text{mol/kg}$  Hapi3 by oral gavage (450 - 560  $\mu\text{L}$  volume range). The rationale for the dose was to test the maximum concentration possible, which was determined by the concentration of the formulation and the volume of the mouse stomach. Formulation preparation is as stated in section 2.7. Briefly, Hapi3 was prepared in 0.5% Solutol® in saline, with or without ball-milling. Due to constraints in drug availability and loss occurring from formulation procedures,

the treatment groups were limited to  $n = 3 - 4$  animals.  $\leq 50 \mu\text{L}$  of blood was collected at various time points by tail vein puncture and larger volumes ( $400 - 600 \mu\text{L}$ ) following euthanasia by cardiac puncture. Following cardiac puncture tissue samples were collected as described in section 2.8. Briefly, tissues were excised, rinsed in saline and frozen. Subsequently, tissue and three volumes water were homogenized with glass dounce and teflon pestle and process as described in section 2.8. Following protein precipitation and centrifugation, samples were analyzed by HPLC as described in section 2.2. Resultant sample AUC values were compared with the corresponding tissue calibration curves shown in Figure 3.2 to determine concentration of Hapi3 in tissue samples.

## **Results and Discussion**

Figure 5.4 shows the resultant plasma concentrations of Hapi3 at various time points following oral administration of either 580, 750 or 1600  $\mu\text{mol/kg}$ . Blue curves represent studies which employed the ball-milled Hapi3 formulation, while curves in red are formulations prepared without ball milling. The largest  $C_{\text{max}}$  was  $55 \pm 6 \mu\text{mol/L}$  and occurred in plasma approximately 1 h following oral administration of 1600  $\mu\text{mol/kg}$  Hapi3. The half life ( $t_{1/2}$ ) of Hapi3 in plasma was approximately 2 h for the study employing 1600  $\mu\text{mol/kg}$  of the ball-milled formulation, however only 1 h for animals given 580  $\mu\text{mol/kg}$  of the non-ball milled formulation. Tissue concentrations at 6 h, graphed as percentage of administered dose, are shown in Figure 5.5. Due to time constraints and scheduling, tumours could not be grown to obtain tumour tissue levels, however muscle tissue levels were used as a proxy.  $\leq 1\%$  of the mean percent administered dose was present in all assayed tissues at 6 h. Figure 5.6 shows muscle

tissue concentrations of Hapi3 at 1, 4 and 6 h following oral gavage of either 750 or 1600  $\mu\text{mol/kg}$  Hapi3. Hapi3  $C_{\text{max}}$  of  $39.3 \pm 6.9 \mu\text{mol/kg}$  ( $n = 3$ ) was observed at 1 h for mice given 750  $\mu\text{mol/kg}$ . At 3 h mean muscle tissue concentration was  $32.2 \pm 9.5 \mu\text{mol/kg}$ . For animals administered 1600  $\mu\text{mol/kg}$  muscle tissue was collected at 6 h for  $n = 4$  mice, with muscle tissue concentrations ranging from 1.3 - 49.9  $\mu\text{mol/kg}$ , indicating highly variable absorption and muscle tissue retention of Hapi3. Sample chromatograms for standards and tissue extracts are shown in Appendix C. Determining Hapi3 concentrations in tissues allowed for some pharmacokinetic and toxicity information to be obtained.

Owing to limited drug availability full pharmacokinetic and clearance studies could not be performed. Tissue and plasma concentrations of the prodrug were assessed while conducting tolerability studies at escalating doses. The amount of raw Hapi3 was limited, to conserve for future experiments, minimal amounts were used for these studies, restricting the number of mice used to 2 - 4 animals per experiment. Dose escalation from 580 to 1600  $\mu\text{mol/kg}$  was possible with the improved ball-milled formulation prepared by the CDRD. Mice appeared unremarkable following p.o. administration of Hapi3, regardless of dose. The absence of observable acute side effects and/or toxicity was a considerable improvement relative to the systemic toxicity reported with repair inhibitors such as wortmannin (66,103).

Ideally a time course would include samples 8 - 24 h following drug administration with a minimum of  $n = 5$  animals at the first half hour and each hourly time point would have been conducted preceding any efficacy work. Due to limited drug availability, drug lost

through formulation, and numerous tolerability studies, a longer time course was not possible. Material was provided to dose six mice. For mice administered 814  $\mu\text{mol/kg}$ , a minimum group number of  $n = 3$  allowed for two time points, 1 and 4 h were chosen.

Highly variable absorption can occur following oral administration of compounds with poor aqueous solubility (104). A high degree of variability was seen in mice given 814  $\mu\text{mol/kg}$  Hapi3 p.o ( $n = 2$ ). Plasma levels of Hapi3  $\pm$  SD were  $19.4 \pm 18.1 \mu\text{mol/L}$  at 5 min post gavage and rose to  $38.5 \pm 11.3 \mu\text{mol/L}$  at 60 min. For oral gavage of 1600  $\mu\text{mol/kg}$ , material sufficient for  $n = 4$  mice was available. While blood was sampled at 60, 180 and 360 min, tissue samples were limited to the experimental end point. Tumour tissue rather than muscle would have been ideal, however equipment failure induced scheduling conflicts between when tumours became available and formulation preparation. Muscle tissue served as a proxy for this reason. Tissue concentrations 6 h post oral administration of 1600  $\mu\text{mol/kg}$  are listed in Table 5.1. These values are highly variable, as means are occasionally double or triple the SD; also, values are either below or very similar to the limit of quantitation ( $1.2 \mu\text{mol/L}$ ) of the assay, indicating a higher degree of sensitivity would be required to detect drug levels at the 6 h time point.

Time is required for the prodrug to diffuse through tissues to reach hypoxic cells and enzymatically release the inhibitor. *In vitro* assays (Minchinton *et al.* unpublished data) suggested that maximal drug conversion occurs  $\sim 2$  h. Examining data points in Figure 5.5, we decided to administer radiation 3 h post drug administration, which would allow time for the prodrug to diffuse and accumulate in tissue moreover allow time for inhibitor release from the prodrug by reductases active in hypoxic cells.

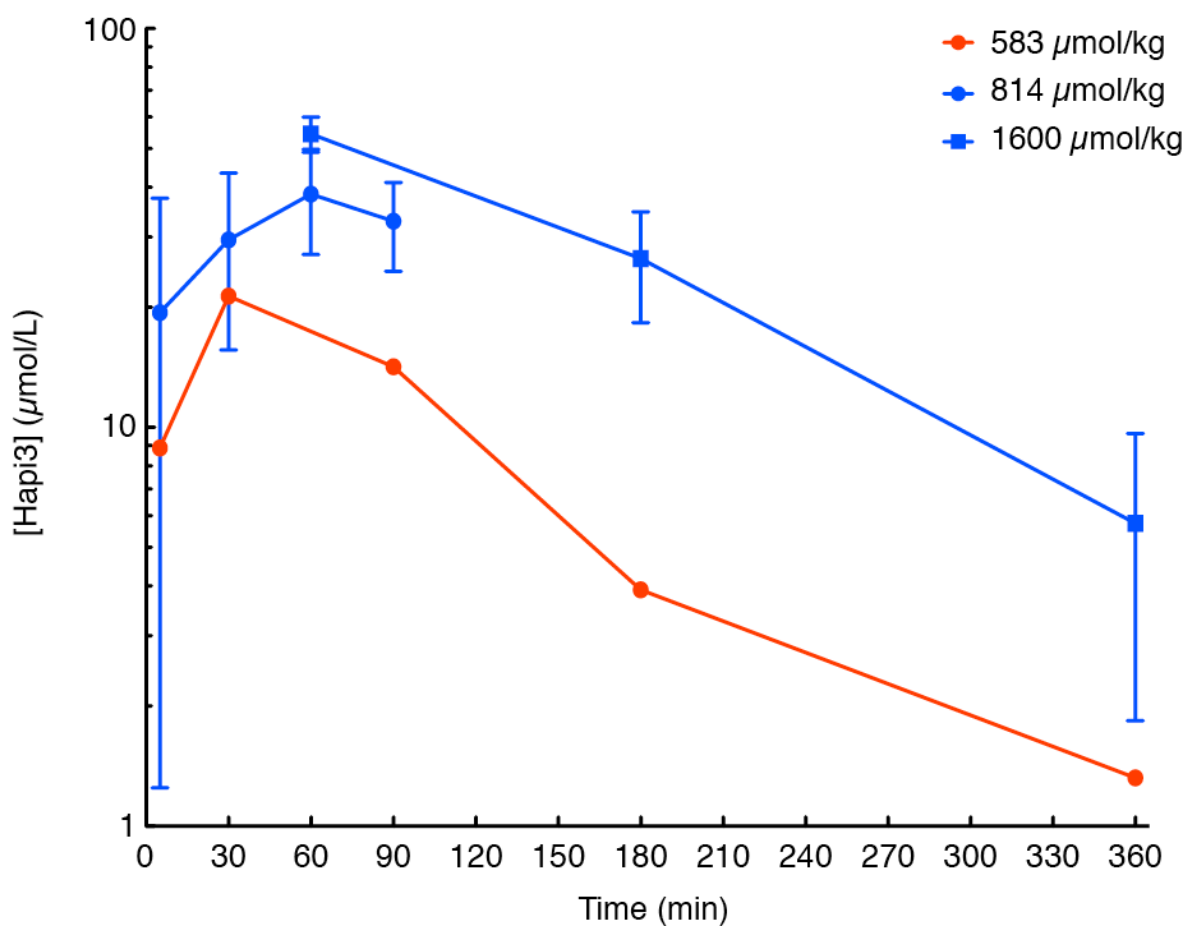


**Figure 5.4 Concentration of Hapi3 in plasma following oral gavage**

The mean concentration ( $\mu\text{mol/L} \pm \text{SD}$ ) of Hapi3 in plasma collected from mice following oral administration of 583  $\mu\text{mol/kg}$ , 814  $\mu\text{mol/kg}$  or 1600  $\mu\text{mol/kg}$  Hapi3. Red, Hapi3 in 0.5% Solutol<sup>®</sup> HS-15/0.9% NaCl; Blue, Hapi3 ball milled in 0.5% Solutol<sup>®</sup> HS-15/0.9% NaCl. All plasma values were above the limit of detection (0.4  $\mu\text{mol/L}$ ) and limit of quantitation (1.2  $\mu\text{mol/L}$ ).



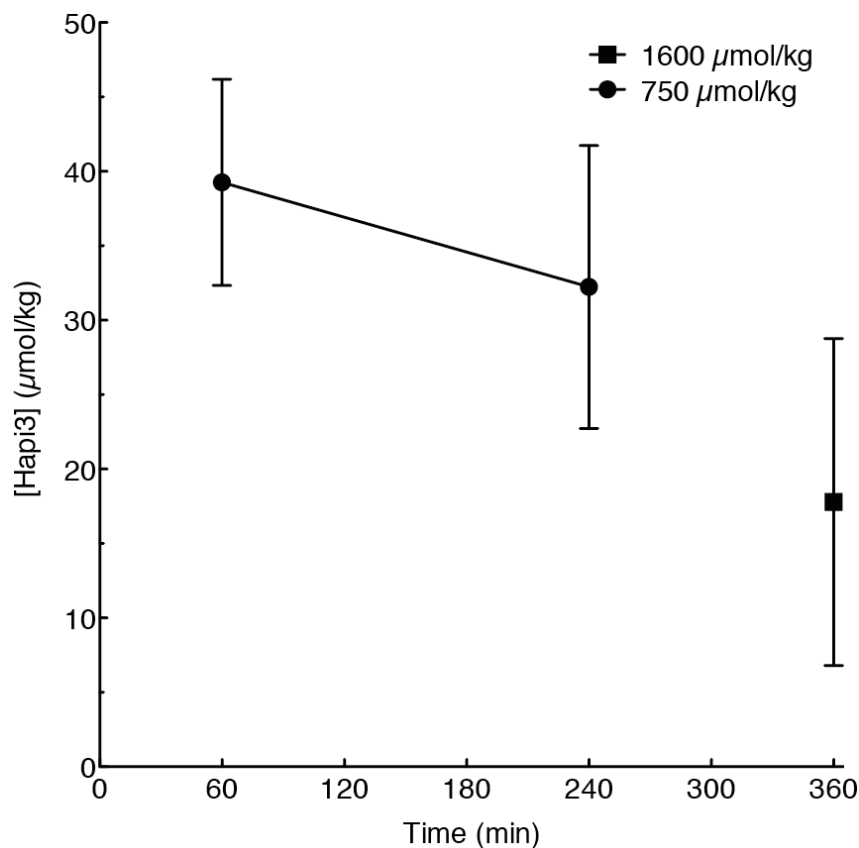


**Figure 5.5 Hapi3 in muscle tissue following oral administration**

The concentration of Hapi3 in tissue samples from mice at 1, 4 or 6 h following oral administration of 750 or 1600  $\mu\text{mol/kg}$  Hapi3 was determined by HPLC. Limited availability of the drug restricted dosing to 3 or 4 mice per time point. Mice administered 750  $\mu\text{mol/kg}$  ( $n = 3$ ) displayed an apparent  $C_{\text{max}}$  in muscle tissue at 1 h of  $39 \pm 7 \mu\text{mol/kg}$ . Muscle tissue of mice administered 1600  $\mu\text{mol/kg}$  ( $n = 4$ ) had  $18 \pm 11 \mu\text{mol/kg}$  at 4 h post oral administration. Mean [Hapi3] in tissue as determined by the linear equation generated by tissue calibration curve in for muscle in Figure 3.2. Muscle values were used as surrogates for tumour tissue. Plotted values are the mean  $\pm$  SEM.

**Table 5.1 Average tissue concentration of Hapi3 6 h post gavage**

Listed is the mean tissue concentration ( $\mu\text{mol/kg} \pm \text{SD}$ ) of Hapi3 tissues 6 h post oral gavage of 1600  $\mu\text{mol/kg}$  Hapi3, ball milled in 0.5% Solutol® HS-15/0.9% NaCl. Tissues were excised, rinsed in cold saline, blotted dry, weighed and frozen. Samples were thawed the following day, kept on ice and processed as described in the materials and methods. Muscle tissue was used as surrogate for tumour tissue.

Plasma	Muscle	Lung	Liver	Kidney	Brain
$5.7 \pm 3.9$	$1.1 \pm 1.4$	$0.95 \pm 0.9$	$1.0 \pm 0.9$	$0.3 \pm 0.3$	$0.0 \pm 0.1$

### **5.3 *In vivo* efficacy studies**

#### **Introduction**

Hapi3 has shown a sensitization enhancement ratio (SER) of 1.8 in hypoxic H460 non-small cell lung carcinoma cells by clonogenic survival (Minchinton et al. unpublished data). Radiosensitization was not observed in oxic (5% O<sub>2</sub>) cells treated with Hapi3. To study efficacy *in vivo*, two tumour xenograft models were chosen which display predominately different forms of hypoxia. HCT116 human colorectal carcinoma cells were chosen as they display more acute or perfusion limited hypoxia. SCCVII murine squamous cell carcinoma cells were chosen for their higher prevalence of chronic or diffusion limited hypoxia. Ideally a small pilot study would have been conducted to determine if a larger dose of fractionated radiotherapy would have been more appropriate than a single large dose. Due to limited quantities of Hapi3 available this could not be done, and a single study with two models was favored.

#### **Approach**

HCT116 (10<sup>7</sup>) or SCCVII (10<sup>6</sup>) cells were subcutaneously implanted into the sacral region of Rag2 mice. When tumours reached an average volume of 200 mm<sup>3</sup>, mice were randomized into treatment groups. Mice received either vehicle alone, radiation alone or radiation in combination with 1600 µmol/kg Hapi3 by oral gavage. Hapi3 was formulated as described in section 2.7. 3 h following gavage, 15 Gy local irradiation was delivered in two equal successive fractions. Mice were monitored daily for apparent signs of toxicity. Tumour volume and animal weight were measured daily for 21 d following initiation of treatment and every 3 d thereafter until tumours reached a maximum volume of 1000 mm<sup>3</sup>.

## Results and Discussion

Administration of the Hapi3 micro-crystalline suspension 3 h prior to radiation treatment produced no statistically significant growth delay over radiation alone in HCT116 human colorectal or SCCVII murine squamous cell carcinoma tumour models. Figure 5.7 displays tumour growth curves for A) HCT116 and B) SCCVII tumour bearing mice. Figure 5.8 summarizes the average mouse weight for A) HCT116 and B) SCCVII tumour bearing mice. No significant weight loss was observed and all treatment groups maintained or increased in body weight over the duration of the experiment.

Tumour growth curves depicted in Figure 5.7 indicate that treatment with Hapi3 3 h prior to local irradiation provided no statistically significant growth delay over radiation alone in either HCT116 or SCCVII xenografts in mice. Limited distribution data for muscle tissue was gathered at 1 and 4 h at a lower dose of 750  $\mu\text{mol/kg}$  ( $n = 3$ ), while 6 h data was obtained for mice administered 1600  $\mu\text{mol/kg}$  ( $n = 4$ ). While larger group numbers as well as extended time points are preferred and necessary for experiments of this nature, limited drug availability as well as an evolving formulation method only permitted small trials. IR was administered 3 h post Hapi3 administration to allow time for Hapi3 to diffuse through tissue and reach hypoxic cells and release the inhibitor as stated above. The growth curve for tumours treated with acute IR in combination with the prodrug was not significantly different relative to the curve of tumours treated with radiation alone.

Failure to observe radiosensitization by the prodrug may be attributed to a variety of factors, such as inability to diffuse and reach hypoxic cells or unfavorable pharmacokinetics. A fractionated radiation regime combined with at least two inhibitor treatments might prove to be a more efficacious approach. Studies by Kashishian *et al.*

(2003) with IC86621 reported a 4 fold growth delay over radiation alone in HCT-116 xenografts grown in BALB/c nude mice(64). In this study IC86621 and radiation were administered in two fractions, with IC86621 injected subcutaneously 1 h before IR and hourly post IR for 3 h. Subcutaneously delivery of the drug presumably by-passed potential problems with absorption and delivery associated with other more conventional modes of administration. Similarly, Shiniohara *et al.* (2005) in collaboration with Kashishian and colleagues published a study in 2005 which reports *in vivo* efficacy of a related flavone-based compound, IC87361(64,65). In this study radiation was given in seven 3 Gy fractions for a total dose of 21 Gy. On days 0 to 4 and days 7 and 8 radiation was given 1 h following i.p. administration of 75  $\mu$ g IC87361. Treatment with IC87361 reduced the fold increase in tumour size relative to radiation alone in both murine Lewis lung carcinoma and B16-F0 melanoma cells grown in C57BL6 mice. An approximate 12 fold increase in tumour growth was delayed by about one week. These studies support the notion that a fractionated approach over a single dose of repair inhibitor and radiation is required to produce a significant xenograft growth delay in mice. The afore mentioned studies also support the position that flavone based compounds present challenges for administration *in vivo* owing to their solubility in aqueous solutions and furthermore, the need of these compounds to be present at the time and in the hours following radiation to observe efficacy. While no significant differences in tumour growth between Hapi3 in combination with radiation over radiation alone, signs of toxicity were not observed by body weight assessment or behaviorally at any point during the experiment (Figures 5.7 and 5.8). Fractionated IR with Hapi3 may

yet produce a growth delay *in vivo*. Further studies are needed to determine a more viable approach.

While radiation and vehicle only controls were used, vehicle plus radiation, drug alone and a positive control would be appropriate for this study. There was insufficient Hapi3 to treat more than 12 mice after various formulation, tolerability and minor pharmacokinetic studies. We previously determined that both HCT116 and SCCVII tumour models would be used, allowing one Hapi3 treatment group (6 animals) per tumour model. If efficacy was displayed, we would pursue generating more robust data with appropriate controls, including drug only. Appropriate positive controls could include known radiosensitizers, such as nimorazole which is currently used clinically in Denmark alone. The DAHANCA 5 study performed in Denmark by Overgaard and colleagues indicates that hypoxic modification with nimorazole improves loco-regional control and produces only minor gastrointestinal toxicity, with few other signs the authors deem as important toxicity (105).

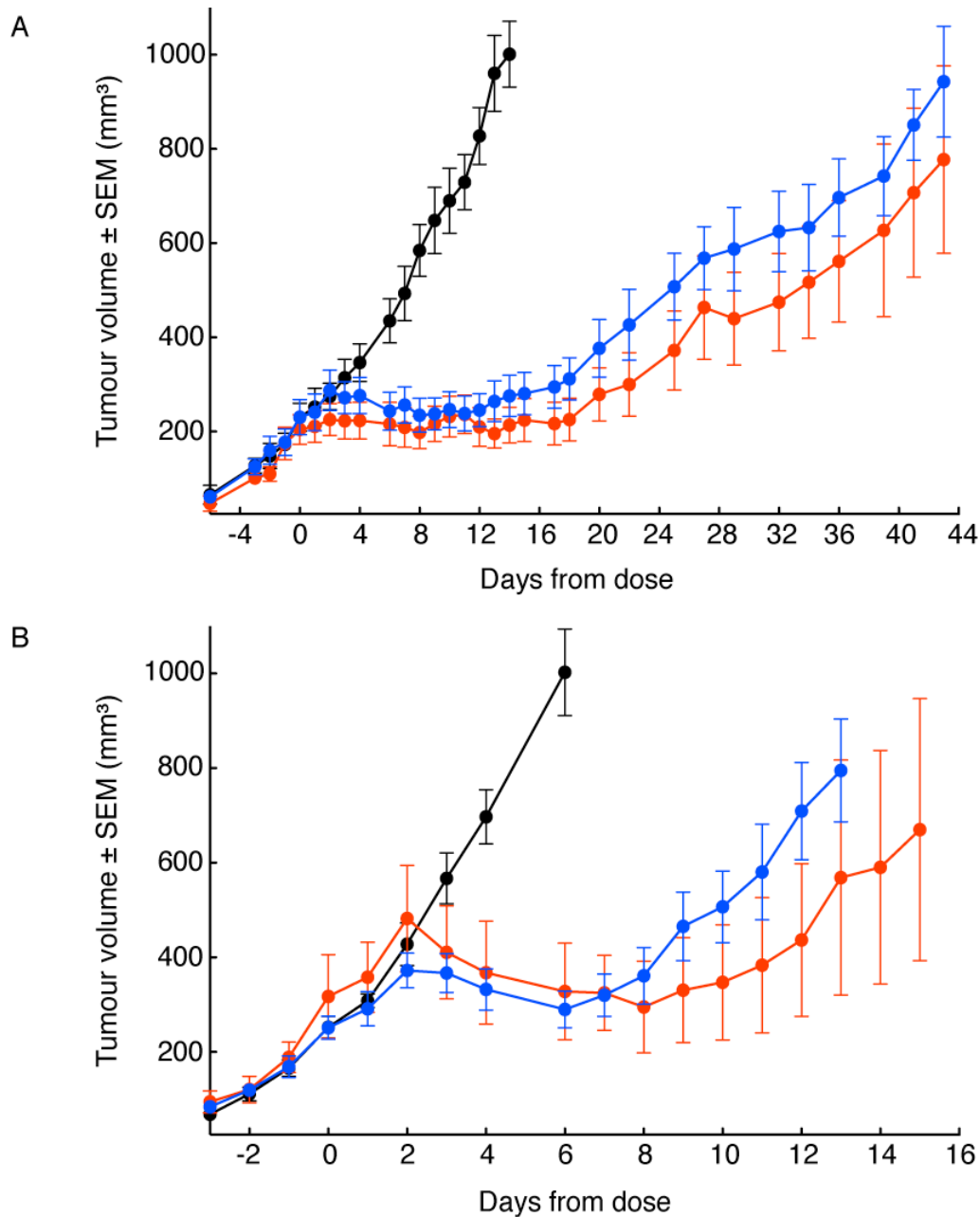


**Figure 5.7 Hapi3 provides no significant additional growth delay over radiation alone**

A) HCT116 xenograft growth in Rag2 mice, un-irradiated vehicle control (black), 15 Gy radiation alone (red), 15 Gy radiation in combination with 1600  $\mu$ mol/kg Hapi3 p.o. Tumour growth in mice treated with Hapi3 3 h prior to receiving IR was not statistically significant compared with mice treated with radiation alone. B) SCCVII xenograft growth in Rag2 mice. Treatment groups as describe above. SCCVII xenografts exhibit predominantly acute hypoxia. Similar to HCT-116, Hapi3 failed to provide any additional growth delay compared with radiation alone.

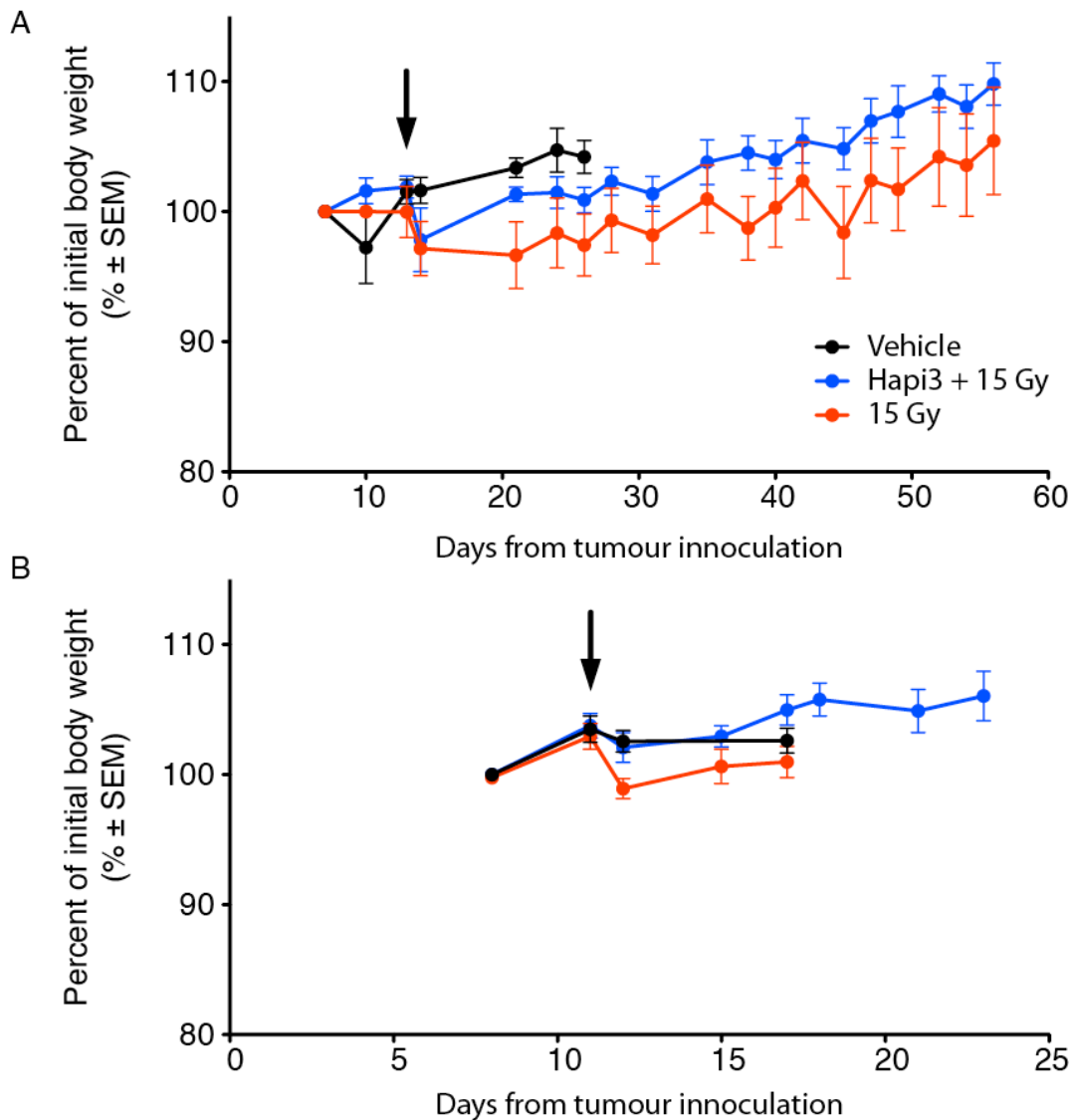


**Figure 5.8 *in vivo* toxicity evaluated by body weight loss**

A) Body weight for HCT-116 bearing mice. All treatment groups maintained or increased in body weight over the duration of the efficacy experiment. Differences were not significant. B) Body weight for SCCVII bearing mice. All treatment groups maintained or increased in body weight over the duration of the efficacy experiment. Differences were not significant. Arrows indicate initiation of treatment.

## Chapter 6: Conclusions and future work

Plasma and tissue concentrations of the prodrug were insufficient to produce radiosensitization *in vivo*. Ball-milling reduce crystal size of the suspension and increased oral bioavailability, however there was no significant difference in tumour growth delay in mice.

While it is unlikely we will continue to develop Hapi3, there are many aspects which deserve further investigation. Improvement chemical synthesis and modification of the prodrug to improve solubility may be possible. Immunohistochemical assessment of features of the tumour microenvironment such as hypoxia, blood vessel distribution and density could determine if the prodrug reaches hypoxic cells. Experimental data regarding the toxicity of HAPs to normal tissues such as bone marrow is scarce in literature. Further investigation into these areas would provide interest and support to the future development of new HAPs.

Future work investigating methods to improve Hapi3 solubility is possible. The addition of a polar, ionizable promoeity . Stella and Nti-Addae (2007) list examples of phosphate ester prodrugs synthesized to improve the bioavailability of poorly soluble drugs(83). The authors also highlight the use of amine groups, which can be protonated to form a water-soluble salt. Liposomal formulations have also been shown to increase solubility and bioavailability of poorly water-soluble compounds (104). However, development of suitable formulations for compounds such as Hapi3, such as customized liposomes, can require significant time, resources and often a large amount of the parent compound (106).



Study of the structure-activity relationships, the relationship between a chemical or 3D structure of a molecule and its biological activity, for the inhibition of DNA-PK have led to the development of more effective DNA-PK inhibitors (107,108). The 3-D crystal structure of DNA-PKcs was difficult to obtain due to the large size of the holoenzyme. However Sibana et al. (2009) reported for the crystal structure of human DNA-PKcs at 6.6 Å resolution (109). The structure presented was the first which allowed for the clear visualization of the overall fold the molecule and active site. This information in combination with advances in bioinformatics, particularly molecular imaging and analysis software could be used to conduct studies to evaluate new candidate inhibitors.

Immunohistochemical analysis of various features of the tumour microenvironment in the hours and days following radiation could provide insight regarding if hypoxic modification occurred. Pimonidazole, a 2-nitroimidazole, is reduced under conditions of cellular hypoxia and becomes complexed to thiol-containing proteins (110). Immunohistochemical quantification of pimonidazole as well as other features of the tumour microenvironment, such as blood vessel distribution and density could be used to provide quantifiable information regarding oxygenation status and tumour physiology at time points following drug administration and radiation. Similarly, tumours could be enzymatically desegregated at time points following treatment and hypoxic fraction could be quantified by fluorescence activated cell sorting. Analysis of this nature would determine if hypoxic cell population within tumours was reduced relative to tumours treated with radiation alone.  $\gamma$ H2AX is a histone modification which is often used for immunocytochemical detection of DSBs (111). Often used in cytology, few examples of  $\gamma$ H2AX in histological section of xenografts or human tumours is present in scientific

literature. In combination with pimonidazole, quantification of  $\gamma$ H2AX could be used to assess the number of induced and sustained DSBs following treatment with Hapi3 in the hypoxic population of solid tumours.

Future work with hypoxia activated DNA repair inhibitors should also include a validated assay to determine the level of released inhibitor present in tumour tissue such that a time course could be performed to determine the optimal schedule for radiation delivery. Also an equally essential question that remains is if a single dose of inhibitor combined with radiation is a suitable treatment regime for repair inhibitors, hypoxia activated or otherwise, for solid tumours *in vivo*.

Relative to other DNA-PK inhibitors with published IC50 values summarized in Table A1, IC86621 is not the most active but is proof of principle that existing DNA-PK inhibitors can be modified with hypoxia activated triggers to generate HAPs which can sensitize cells to IR.

Aside from good aqueous solubility, new candidate HAP repair inhibitors should be evaluated for tissue diffusion before beginning *in vivo* studies. Drug diffusion can be studied with multi-layered cell culture models or spheroid cell culture models, however these approaches do not account for first pass metabolism by the liver and may require large amounts of drug which can be an obstacle during development. An ideal candidate would be present in sufficient concentration in the tumour at the time of radiation to inhibit repair in hypoxic cells and remain at a sufficient concentration in the hours following radiation while a majority of repair occurs.

Toxicity to the bone marrow is also another important area requiring assessment for HAP DNA repair inhibitors. The bone marrow is suspected to contain regions of hypoxia and may suffer adverse side effects from repair inhibition (112). Clonogenic survival of bone marrow stem cells should be performed in order to assess *in vivo* toxicity for HAP DNA repair inhibitors in the future. Similarly, serum levels of creatinine and liver transaminases could be assayed to assess liver toxicity. These techniques may provide early insight regarding potential toxicity for repair inhibition particularly when combined with other therapeutics.

These experiments combined with work by Kirtsin E. Lindquist and unpublished data from our group are proof of principle that hypoxic modification of known inhibitors can result in the release of the inhibitor selectively in hypoxic environments resulting in selective radiosensitization.

## References

1. Lindquist K. THE DEVELOPMENT OF HYPOXIA ACTIVATED DNA REPAIR INHIBITORS. Minchinton A, editor. [Vancouver, BC]: University of British Columbia; 2009. pages 1–88.
2. Delaney G, Jacob S, Featherstone C, Barton M. The role of radiotherapy in cancer treatment. *Cancer*. 2005;104:1129–37.
3. Begg AC, Stewart FA, Vens C. Strategies to improve radiotherapy with targeted drugs. *Nat. Rev. Cancer*. 2011;11:239–53.
4. Harada H. How can we overcome tumor hypoxia in radiation therapy? *J. Radiat. Res*. 2011;52:545–56.
5. Chatterjee A, Magee JL, Dey SK. The role of homogeneous reactions in the radiolysis of water. *Radiation Research*. Academic Press, Inc; 1983;96:1–19.
6. Roots R, Okada S. Estimation of life times and diffusion distances of radicals involved in X-ray-induced DNA strand breaks or killing of mammalian cells. *Radiation Research*. Academic Press, Inc; 1975;64:306–20.
7. Friedberg EC, Walker GC, Siede W. DNA repair and mutagenesis. Amer Society for Microbiology; 1995.
8. Mladenov E, Iliakis G. Induction and repair of DNA double strand breaks: The increasing spectrum of non-homologous end joining pathways. *Mutat. Res*. 2011;711:61–72.
9. Hall EJ, Giaccia AJ. *Radiobiology for the Radiologist*, 6e. 6th ed. Lippincott Williams&Wilki; 2006;:546.
10. Brown J. The Hypoxic Cell. *Cancer Res*. 1999.
11. Vaupel P, Höckel M. Tumor hypoxia and therapeutic resistance. Recombinant Human Erythropoietin (rhEPO) in clinical oncology. Springer; 2008;:283–305.
12. Franko AJ, Sutherland RM. Radiation survival of cells from spheroids grown in different oxygen concentrations. *Radiation Research*. 1979;79:454–67.
13. Hammond EM, Olcina M, Giaccia AJ. Hypoxia and Modulation of Cellular Radiation Response. In: DeWeese TL, Laiho M, editors. *Molecular Determinants of Radiation Response*, Current Cancer Research. Springer Science+Business Media; page 276.

14. Gray L, Conger A, Ebert M, Hornsey S, Scott O. The concentration of oxygen dissolved in tissues at the time of irradiation as a factor in radiotherapy. *Br J Radiol.* 1953;26:638–48.
15. Brown JM, Wilson WR. Exploiting tumour hypoxia in cancer treatment. *Nat. Rev. Cancer.* Nature Publishing Group; 2004;4:437–47.
16. Thomlinson RH, Gray L. The histological structure of some human lung cancers and the possible implications for radiotherapy. *Br. J. Cancer.* 1955;9:539–49.
17. Primeau AJ, Rendon A, Hedley D, Lilge L, Tannock IF. The distribution of the anticancer drug Doxorubicin in relation to blood vessels in solid tumors. *Clin. Cancer Res.* 2005;11:8782–8.
18. Kyle AH, Huxham LA, Yeoman DM, Minchinton AI. Limited Tissue Penetration of Taxanes: A Mechanism for Resistance in Solid Tumors. *Clinical Cancer Research.* 2007;13:2804–10.
19. Kyle AH, Baker JHE, Minchinton AI. Targeting Quiescent Tumor Cells via Oxygen and IGF-I Supplementation. *Cancer Res.* 2012.
20. Brown JM. Evidence for acutely hypoxic cells in mouse tumours, and a possible mechanism of reoxygenation. *Br J Radiol.* 1979;52:650–6.
21. Chaplin DJ, Olive PL, Durand RE. Intermittent blood flow in a murine tumor: radiobiological effects. *Cancer Res.* 1987;47:597–601.
22. Dewhirst MW, Braun RD, Lanzen JL. Temporal changes in PO<sub>2</sub> of R3230AC tumors in Fischer-344 rats. *Int. J. Radiat. Oncol. Biol. Phys.* 1998;42:723–6.
23. Vaupel P, Harrison L. Tumor hypoxia: causative factors, compensatory mechanisms, and cellular response. *Oncologist.* 2004;9 Suppl 5:4–9.
24. Minchinton AI, Tannock IF. Drug penetration in solid tumours. *Nat. Rev. Cancer.* 2006;6:583–92.
25. Höckel M, Schlenger K, Knoop C, Vaupel P. Oxygenation of Carcinomas of the Uterine Cervix: Evaluation by Computerized O<sub>2</sub> Tension Measurements. *Cancer Res.* 1991.
26. Höckel M, Vorndran B, Schlenger K, Baussmann E, Knapstein PG. Tumor oxygenation: a new predictive parameter in locally advanced cancer of the uterine cervix. *Gynecol. Oncol.* 1993;51:141–9.
27. Höckel M, Schlenger K, Mitze M, Schäffer U, Vaupel P. Hypoxia and Radiation Response in Human Tumors. *Semin Radiat Oncol.* 1996;6:3–9.

28. Moeller BJ, Richardson RA, Dewhirst MW. Hypoxia and radiotherapy: opportunities for improved outcomes in cancer treatment. *Cancer Metastasis Rev.* 2007;26:241–8.
29. Sullivan DM, Glisson BS, Hodges PK, Smallwood-Kentro S, Ross WE. Proliferation dependence of topoisomerase II mediated drug action. *Biochemistry.* 1986;25:2248–56.
30. Chabner BA, Eds BCK, Brunton LL. Goodman & Gilman's The Pharmacological Basis of Therapeutics, 12e. 12(null) ed. McGraw Hill. New York.
31. Minchinton AI, Kyle AH. Drug Penetration and Therapeutic Resistance. In: Siemann DW, editor. *Tumor Microenvironment.* 1st ed. John Wiley & Sons, Ltd; 2011. pages 328–52.
32. Höckel M, Vaupel P. Tumor Hypoxia: Definitions and Current Clinical, Biologic, and Molecular Aspects. *JNCI Journal of the National Cancer Institute.* 2001;93:266–76.
33. Adams G. Hypoxic cell sensitizers for radiotherapy. Multiple values selected. 1978;4:135–41.
34. Chapman J, Reuvers A, Borsa J, Petkau A. Nitrofurans as Radiosensitizers of Hypoxic Mammalian Cells. *Cancer Res.* 1972.
35. Franko AJ, Koch CJ, Boisvert DP. Distribution of misonidazole adducts in 9L gliosarcoma tumors and spheroids: implications for oxygen distribution. *Cancer Res.* 1992;52:3831–7.
36. Oronsky BT, Knox SJ, Scicinski J. Six degrees of separation: the oxygen effect in the development of radiosensitizers. *Transl Oncol.* 2011;4:189–98.
37. Overgaard J, Horsman MR. Modification of hypoxia-induced radioresistance in tumors by the use of oxygen and sensitizers. *Semin Radiat Oncol.* Elsevier; 1996;6:10–21.
38. Dugle DL, Gillespie CJ, Chapman JD. DNA strand breaks, repair, and survival in x-irradiated mammalian cells. *Proc. Natl. Acad. Sci. U.S.A.* 1976;73:809–12.
39. Lees-Miller SP, Meek K. Repair of DNA double strand breaks by non-homologous end joining. *Biochimie.* 2003;85:1161–73.
40. Pfeiffer P, Goedecke W, Kuhfittig-Kulle S, Obe G. Pathways of DNA double-strand break repair and their impact on the prevention and formation of chromosomal aberrations. *Cytogenet Genome Res.* 2004;104:7–13.
41. Khanna K, Jackson S. DNA double-strand breaks: signaling, repair and the cancer connection. *Nat. Genet.* 2001;27:247–54.
42. Helleday T, Lo J, van Gent DC, Engelward BP. DNA double-strand break repair: from mechanistic understanding to cancer treatment. *DNA Repair.* 2007;6:923–35.

43. Jeggo PA. Identification of genes involved in repair of DNA double-strand breaks in mammalian cells. *Radiation Research*. 1998;150:S80–91.
44. Brnzei D, Foiani M. Regulation of DNA repair throughout the cell cycle. *Nat Rev Mol Cell Biol*. Nature Publishing Group; 2008;9:297–308.
45. Blier PR, Griffith AJ, Craft J, Hardin JA. Binding of Ku protein to DNA. Measurement of affinity for ends and demonstration of binding to nicks. *J. Biol. Chem*. 1993;268:7594–601.
46. Mimori T, Hardin JA. Mechanism of interaction between Ku protein and DNA. *J. Biol. Chem*. 1986;261:10375–9.
47. Walker JR, Corpina RA, Goldberg J. Structure of the Ku heterodimer bound to DNA and its implications for double-strand break repair. *nature*. 2001;412:607–14.
48. Biedermann KA, Sun JR, Giaccia AJ, Tosto LM, Brown JM. scid mutation in mice confers hypersensitivity to ionizing radiation and a deficiency in DNA double-strand break repair. *Proc. Natl. Acad. Sci. U.S.A*. 1991;88:1394–7.
49. Kurimasa A, Kumano S, Boubnov NV, Story MD, Tung CS, Peterson SR, et al. Requirement for the kinase activity of human DNA-dependent protein kinase catalytic subunit in DNA strand break rejoining. *Mol. Cell. Biol*. 1999;19:3877–84.
50. Chan DW, Chen BP-C, Prithivirajsingh S, Kurimasa A, Story MD, Qin J, et al. Autophosphorylation of the DNA-dependent protein kinase catalytic subunit is required for rejoining of DNA double-strand breaks. *Genes Dev*. 2002;16:2333–8.
51. Cho Y, Lees-Miller S, Meek K. Autophosphorylation of DNA-Dependent Protein Kinase Regulates DNA End Processing and May Also Alter Double-Strand Break Repair Pathway Choice. ... and cellular biology. 2005.
52. Convery E, Shin EK, Ding Q, Wang W, Douglas P, Davis LS, et al. Inhibition of homologous recombination by variants of the catalytic subunit of the DNA-dependent protein kinase (DNA-PKcs). *Proc. Natl. Acad. Sci. U.S.A*. 2005;102:1345–50.
53. Lieber MR. The Mechanism of Double-Strand DNA Break Repair by the Nonhomologous DNA End-Joining Pathway. *Annu. Rev. Biochem*. 2010;79:181–211.
54. Weterings E, Chen DJ. The endless tale of non-homologous end-joining. *Cell Res*. Nature Publishing Group; 2008;18:114–24.
55. Helleday T, Petermann E, Lundin C, Hodgson B, Sharma RA. DNA repair pathways as targets for cancer therapy. *Nat. Rev. Cancer*. 2008;8:193–204.
56. Arcaro A, Wymann MP. Wortmannin is a potent phosphatidylinositol 3-kinase inhibitor: the role of phosphatidylinositol 3,4,5-trisphosphate in neutrophil responses. *Biochem. J*. Portland Press Ltd; 1993;296:297.

57. Rosenzweig KE, Youmell MB, Palayoor ST, Price BD. Radiosensitization of human tumor cells by the phosphatidylinositol3-kinase inhibitors wortmannin and LY294002 correlates with inhibition of DNA-dependent protein kinase and prolonged G2-M delay. *Clin. Cancer Res.* 1997;3:1149–56.
58. Ihle NT, Williams R, Chow S, Chew W, Berggren MI, Paine-Murrieta G, et al. Molecular pharmacology and antitumor activity of PX-866, a novel inhibitor of phosphoinositide-3-kinase signaling. *Mol. Cancer Ther.* 2004;3:763–72.
59. Veuger S, Curtin N, Richardson C, Smith G. Radiosensitization and DNA Repair Inhibition by the Combined Use of Novel Inhibitors of DNA-dependent Protein Kinase and Poly(ADP-Ribose) Polymerase-1. *Cancer Res.* 2003.
60. Veuger SJ, Curtin NJ, Smith GCM, Durkacz BW. Effects of novel inhibitors of poly(ADP-ribose) polymerase-1 and the DNA-dependent protein kinase on enzyme activities and DNA repair. *Oncogene.* 2004;23:7322–9.
61. Nutley BP, Smith NF, Hayes A, Kelland LR, Brunton L, Golding BT, et al. Preclinical pharmacokinetics and metabolism of a novel prototype DNA-PK inhibitor NU7026. *Br. J. Cancer.* 2005;93:1011–8.
62. Leahy JJJ, Golding BT, Griffin RJ, Hardcastle IR, Richardson C, Rigoreau L, et al. Identification of a highly potent and selective DNA-dependent protein kinase (DNA-PK) inhibitor (NU7441) by screening of chromenone libraries. *Bioorg. Med. Chem. Lett.* 2004;14:6083–7.
63. Li P, Zhao L. Developing early formulations: practice and perspective. *Int J Pharm.* 2007;341:1–19.
64. Kashishian A, Douangpanya H, Clark D, Schlachter ST, Eary CT, Schiro JG, et al. DNA-dependent protein kinase inhibitors as drug candidates for the treatment of cancer. *Mol. Cancer Ther.* 2003;2:1257–64.
65. Shinohara ET, Geng L, Tan J, Chen H, Shir Y, Edwards E, et al. DNA-dependent protein kinase is a molecular target for the development of noncytotoxic radiation-sensitizing drugs. *Cancer Res.* 2005;65:4987–92.
66. Karve S, Werner ME, Sukumar R, Cummings ND, Copp JA, Wang EC, et al. Revival of the abandoned therapeutic wortmannin by nanoparticle drug delivery. 2012.
67. Denny WA. The role of hypoxia-activated prodrugs in cancer therapy. *Lancet Oncol.* 2000;1:25–9.
68. Huttunen KM, Raunio H, Rautio J. Prodrugs—from Serendipity to Rational Design. *Pharmacol. Rev.* 2011.
69. Rautio J, Kumpulainen H, Heimbach T, Oliyai R, Oh D, Järvinen T, et al. Prodrugs: design and clinical applications. *Nat Rev Drug Discov.* 2008;7:255–70.



70. Wilson WR, Hay MP. Targeting hypoxia in cancer therapy. *Nat. Rev. Cancer*. 2011.
71. Denny WA, Wilson WR, Hay MP. Recent developments in the design of bio-reductive drugs. *The British Journal of Cancer. Supplement*. 1996;27:S32–8.
72. Naylor MA, Thomson P. Recent advances in bio-reductive drug targeting. *Mini reviews in medicinal chemistry*. Bentham Science Publishers; 2001;1:17–29.
73. Failes TW, Hambley TW. Models of hypoxia activated prodrugs: Co(III) complexes of hydroxamic acids. *Dalton Trans*. 2006;:1895.
74. JB S, Lu GL, Van Leeuwen W, Abbattista M. Design and identification of the novel hypoxia-activated irreversible pan-HER inhibitor SN 29966. *AACR Annual Meeting*. AACR Annual Meeting; 2009.
75. Yuan F, Quan L-D, Cui L, Goldring SR, Wang D. Development of macromolecular prodrug for rheumatoid arthritis. *Adv. Drug Deliv. Rev*. 2012;64:1205–19.
76. Hart CP, Sun JD, Liu Q, Ammons S, Lister D. Efficacy of the hypoxia-activated prodrug TH-302 in a preclinical model of prostate cancer metastasis. *Oncol*. 1999.
77. Bhupathi D, Curd JG, Matteucci MD, Hart CP. Hypoxia-Dependent In Vivo Activity of the Hypoxia-Activated Prodrug (HAP) TH-302.  
. Orlando, Florida.
78. Lipinski C. Poor Aqueous Solubility-an Industry Wide Problem in ADME Screening. *American Pharmaceutical Review*. 2002.
79. Rabinow BE. Nanosuspensions in drug delivery. *Nat Rev Drug Discov*. 2004;3:785–96.
80. Stegemann S, Leveiller F, Franchi D, de Jong H, Lindén H. When poor solubility becomes an issue: From early stage to proof of concept. *European Journal of Pharmaceutical Sciences*. 2007;31:249–61.
81. Venkatesh S, Lipper RA. Role of the development scientist in compound lead selection and optimization. *J Pharm Sci*. 2000;89:145–54.
82. Ohara T, Kitamura S, Kitagawa T, Terada K. Dissolution mechanism of poorly water-soluble drug from extended release solid dispersion system with ethylcellulose and hydroxypropylmethylcellulose. *Int J Pharm*. 2005;302:95–102.
83. Stella VJ, Nti-Addae KW. Prodrug strategies to overcome poor water solubility. *Adv. Drug Deliv. Rev*. 2007;59:677–94.
84. Leuner C, Dressman J. Improving drug solubility for oral delivery using solid dispersions. *Eur J Pharm Biopharm*. 2000;50:47–60.

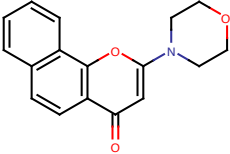
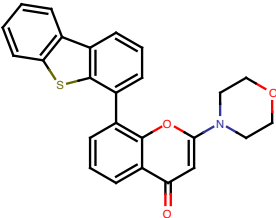
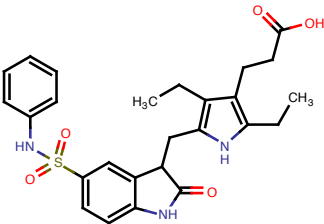
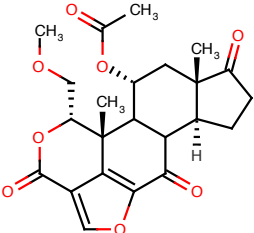
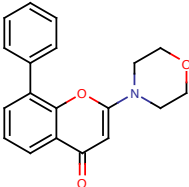
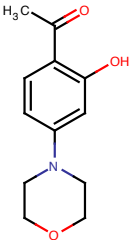
85. Strickley RG. Solubilizing excipients in oral and injectable formulations. *Pharm. Res.* 2004;21:201–30.
86. Serajuddin ATM, Sheen P-C, Mufson D, Bernstein DF, Augustine MA. Effect of vehicle amphiphilicity on the dissolution and bioavailability of a poorly water-soluble drug from solid dispersions. *J Pharm Sci.* Wiley Subscription Services, Inc., A Wiley Company; 1988;77:414–7.
87. Ghosh I, Bose S, Vippagunta R, Harmon F. Nanosuspension for improving the bioavailability of a poorly soluble drug and screening of stabilizing agents to inhibit crystal growth. *Int J Pharm.* 2011;409:260–8.
88. Kesisoglou F, Panmai S, Wu Y. Nanosizing--oral formulation development and biopharmaceutical evaluation. *Adv. Drug Deliv. Rev.* 2007;59:631–44.
89. Van Eerdenbrugh B, Van den Mooter G, Augustijns P. Top-down production of drug nanocrystals: Nanosuspension stabilization, miniaturization and transformation into solid products. *Int J Pharm.* 2008;364:64–75.
90. Luitpold Pharmaceuticals, Inc. Materials and methods to potentiate cancer treatment. US Patent Office; 2007.
91. Matuszewski BK, Constanzer ML, Chavez-Eng CM. Strategies for the Assessment of Matrix Effect in Quantitative Bioanalytical Methods Based on HPLC–MS/MS. *Anal. Chem.* 2003;75:3019–30.
92. Bishop EJ, Kou D, Manius G, Chokshi HP. Sample Preparation of Pharmaceutical Dosage Forms. Nickerson B, editor. Boston, MA: Springer US; 2011. pages 233–51.
93. Müller CE. Prodrug approaches for enhancing the bioavailability of drugs with low solubility. *Chem. Biodivers.* 2009;6:2071–83.
94. Friedrich H, Fussnegger B, Kolter K, Bodmeier R. Dissolution rate improvement of poorly water-soluble drugs obtained by adsorbing solutions of drugs in hydrophilic solvents onto high surface area carriers. *European Journal of Pharmaceutics and Biopharmaceutics.* 2006;62:171–7.
95. Anoopkumar-Dukie S, Carey JB, Conere T, O'sullivan E, van Pelt FN, Allshire A. Resazurin assay of radiation response in cultured cells. *Br J Radiol.* 2005;78:945–7.
96. Czekanska EM. Assessment of cell proliferation with resazurin-based fluorescent dye. Czekanska EM, editor. *Methods Mol. Biol.* Totowa, NJ; 2011;740:27–32.
97. Gonzalez RJ, Tarloff JB. Evaluation of hepatic subcellular fractions for Alamar blue and MTT reductase activity. *Toxicology in Vitro.* 2001;15:257–9.

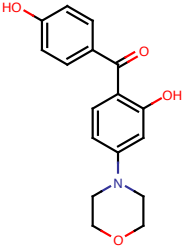
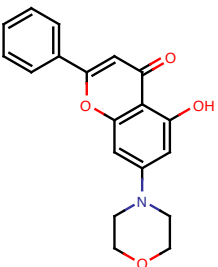
98. Finnie NJ, Gottlieb TM, Blunt T, Jeggo PA, Jackson SP. DNA-dependent protein kinase activity is absent in xrs-6 cells: implications for site-specific recombination and DNA double-strand break repair. *Proc. Natl. Acad. Sci. U.S.A.* 1995;92:320–4.
99. Lees-Miller SP, Chen YR, Anderson CW. Human cells contain a DNA-activated protein kinase that phosphorylates simian virus 40 T antigen, mouse p53, and the human Ku autoantigen. *Mol. Cell. Biol. Am Soc Microbiol*; 1990;10:6472–81.
100. Kühne M, Riballo E, Rief N, Rothkamm K, Jeggo PA, Löbrich M. A double-strand break repair defect in ATM-deficient cells contributes to radiosensitivity. *Cancer Res.* 2004;64:500–8.
101. Riballo E, Kühne M, Rief N, Doherty A, Smith GCM, Recio M-J, et al. A pathway of double-strand break rejoining dependent upon ATM, Artemis, and proteins locating to gamma-H2AX foci. *Mol. Cell.* 2004;16:715–24.
102. Nevaldine B, Longo JA, Hahn PJ. The scid defect results in much slower repair of DNA double-strand breaks but not high levels of residual breaks. *Radiation Research. Radiation Research Society*; 1997;147:535–40.
103. Sarkaria J, Tibbetts R, Busby E, Kennedy A. Inhibition of Phosphoinositide 3-Kinase Related Kinases by the Radiosensitizing Agent Wortmannin. *Cancer Res.* 1998.
104. van Hoogevest P, Liu X, Fahr A. Drug delivery strategies for poorly water-soluble drugs: the industrial perspective. *Expert Opin Drug Deliv.* 2011;8:1481–500.
105. Overgaard J, Hansen HS, Overgaard M, Bastholt L, Berthelsen A, Specht L, et al. A randomized double-blind phase III study of nimorazole as a hypoxic radiosensitizer of primary radiotherapy in supraglottic larynx and pharynx carcinoma. Results of the Danish Head and Neck Cancer Study (DAHANCA) Protocol 5-85. *Radiother Oncol.* 1998;46:135–46.
106. Dai W-G, Dong LC, Li S, Pollock-Dove C, Chen J, Mansky P, et al. Parallel screening approach to identify solubility-enhancing formulations for improved bioavailability of a poorly water-soluble compound using milligram quantities of material. *Int J Pharm.* 2007;336:1–11.
107. Hardcastle IR, Cockcroft X, Curtin NJ, El-Murr MD, Leahy JJJ, Stockley M, et al. Discovery of Potent Chromen-4-one Inhibitors of the DNA-Dependent Protein Kinase (DNA-PK) Using a Small-Molecule Library Approach - *Journal of Medicinal Chemistry (ACS Publications).* *J. Med. Chem.* 2005;48:7829–46.
108. Clapham KM, Bardos J, Finlay MRV, Golding BT, Griffen EJ, Griffin RJ, et al. DNA-dependent protein kinase (DNA-PK) inhibitors: structure-activity relationships for O-alkoxyphenylchromen-4-one probes of the ATP-binding domain. *Bioorg. Med. Chem. Lett.* 2011;21:966–70.

109. Sibanda BL, Chirgadze DY, Blundell TL. Crystal structure of DNA-PKcs reveals a large open-ring cradle comprised of HEAT repeats. *nature*. 2009;463:118–21.
110. Varia MA, Calkins-Adams DP, Rinker LH, Kennedy AS, Novotny DB, Fowler WC, et al. Pimonidazole: a novel hypoxia marker for complementary study of tumor hypoxia and cell proliferation in cervical carcinoma. *Gynecol. Oncol.* 1998;71:270–7.
111. Bonner WM, Redon CE, Dickey JS, Nakamura AJ, Sedelnikova OA, Solier S, et al.  $\gamma$ H2AX and cancer. *Nat. Rev. Cancer*. Nature Publishing Group; 2008;8:957–67.
112. Parmar K, Mauch P, Vergilio J-A, Sackstein R, Down JD. Distribution of hematopoietic stem cells in the bone marrow according to regional hypoxia. *Proc. Natl. Acad. Sci. U.S.A.* 2007;104:5431–6.

# Appendices

## Appendix A: Chemical structures of various DNA-PK inhibitors

Compound	Structure	IC50 (nm) for DNA-PK	Reference
NU7026		230	57
NU7441		14	58
SU11752		130	107
Wortmannin		150	60
LY294002		360	60
IC86621		120	60

IC87102		35	60
IC87361		34	60

## Appendix B: Tissue extraction of Hapi3 sample calculation of percent recovery

Tissue homogenate was spiked with a stock solution of Hapi3 in DMSO such that the final concentration of Hapi3 was 0.5, 2, 5, 10 or 20  $\mu\text{mol/L}$ . Hapi3 was extracted from the homogenate with an equal volume of 6%  $\text{ZnSO}_4$  in methanol, which increased the final volume of the sample by a factor of 2. Tissue calibration curves shown in Figure 3.2 plot the concentration in homogenate relative to the area under the curve of the extracted sample. Values extrapolated from the curve must be multiplied by a factor of two to obtain the correct tissue concentration. As such the slope of the tissue calibration curves are approximately half that of the standard in methanol/6%  $\text{ZnSO}_4$ .

For muscle tissue spiked with 5  $\mu\text{mol/L}$  Hapi3, extract HPLC A.U.C values were:

$$n1 = 11237$$

$$n2 = 11762$$

$$n3 = 10963$$

$$\text{mean A.U.C.} = 11320.7$$

Linear equation obtained from curve constructed in MeOH/6%  $\text{ZnSO}_4$ :

$$y = 4964.9x - 2290.9$$

$$(2 * 11320.7) = 4964.9x - 2290.9 \quad (\text{sample value is multiplied by 2 to account for dilution})$$

$$x = (11320.7 + 2290.9)/4964.9$$

To give percent recovery, divide value obtained by actual amount present (5  $\mu\text{mol/L}$ ) and multiply by 100:

$$x = 5.02/5.00 * 100 = 100.4 \% \text{ recovery}$$

Mean percent recovery values were calculated for all each point of the calibration curve, averaged and the mean  $\pm$  the SD is shown in Table 3.2



## Appendix C: HPLC sample chromatograms

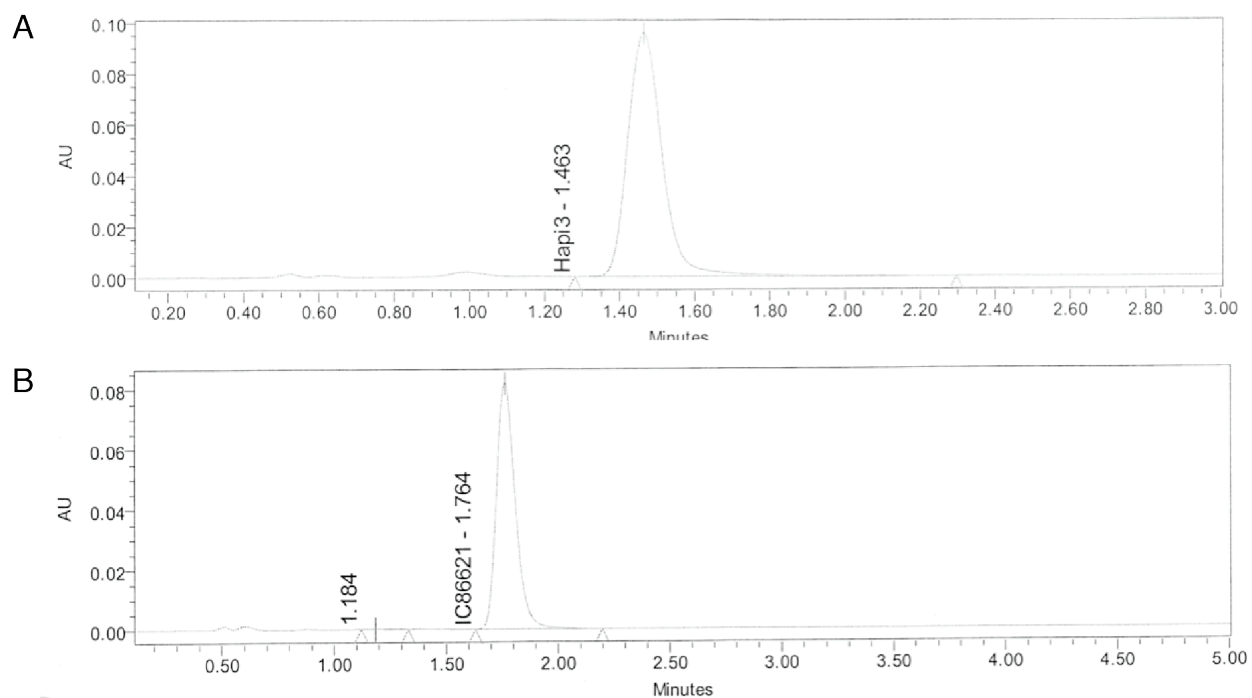


**Figure A1 HPLC chromatograms of external standards Hapi3 and IC86621**

All injections were performed as described in materials and methods section 2.2. All curves show absorbance units detected relative to time measured at either 320 nm (Hapi3) or 340 nm (IC86621). A) 150  $\mu\text{mol/L}$  Hapi3. B) 100  $\mu\text{mol/L}$  IC86621.

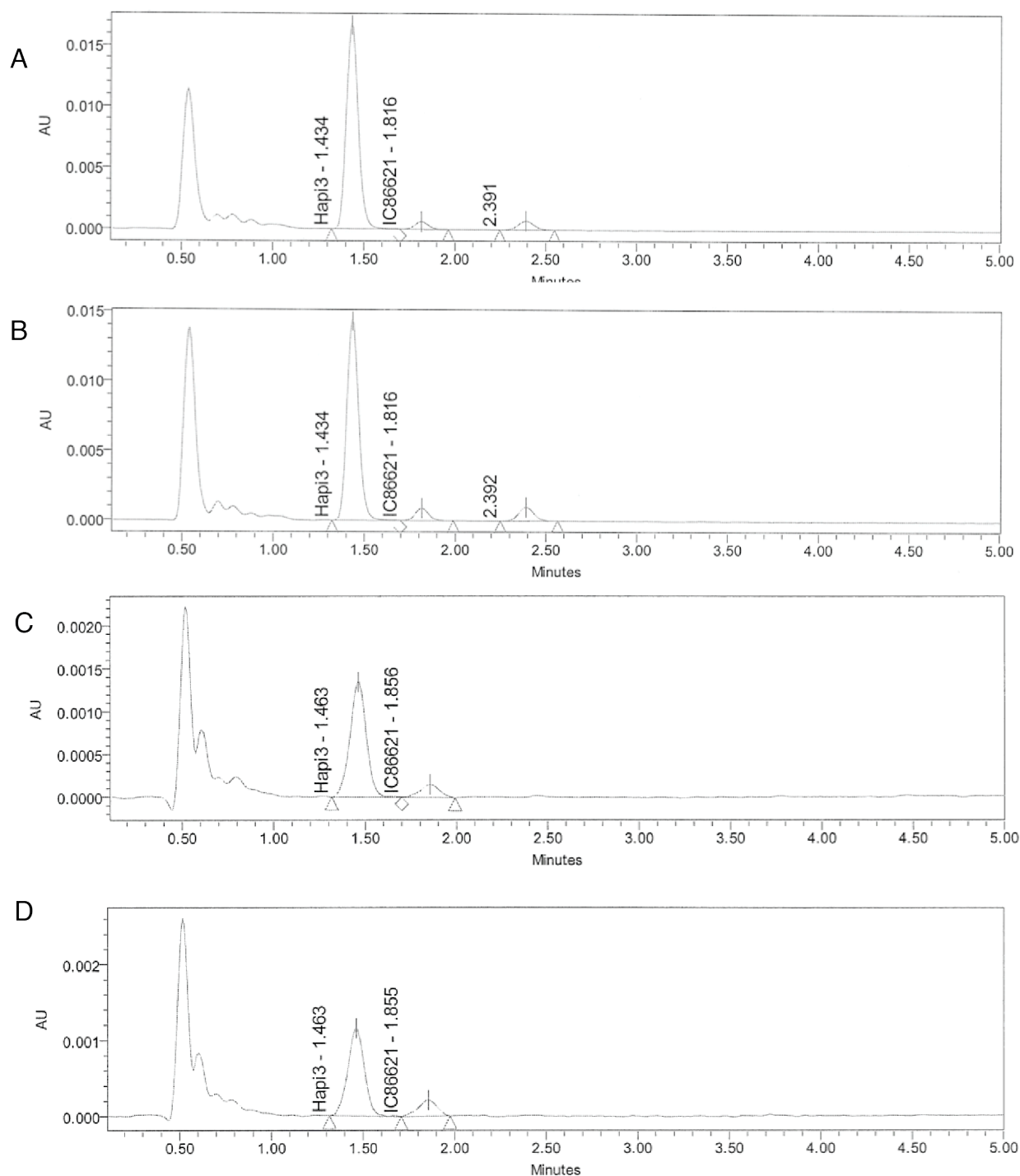


**Figure A2 HPLC chromatograms of plasma and heart extracts**

Chromatograms from resultant plasma and heart tissue extracts 4 h following p.o. administration of 814  $\mu\text{mol/L}$  Hapi3. All injections were performed as described in materials and methods section 2.2. A) Plasma, 320 nm. B) Plasma, 340 nm. C) Heart, 320 nm D) Heart, 340 nm. Unlabeled peaks are possibly unidentified metabolites. Hapi3 was detected at 320 nm, IC86621 was detected at 340 nm.

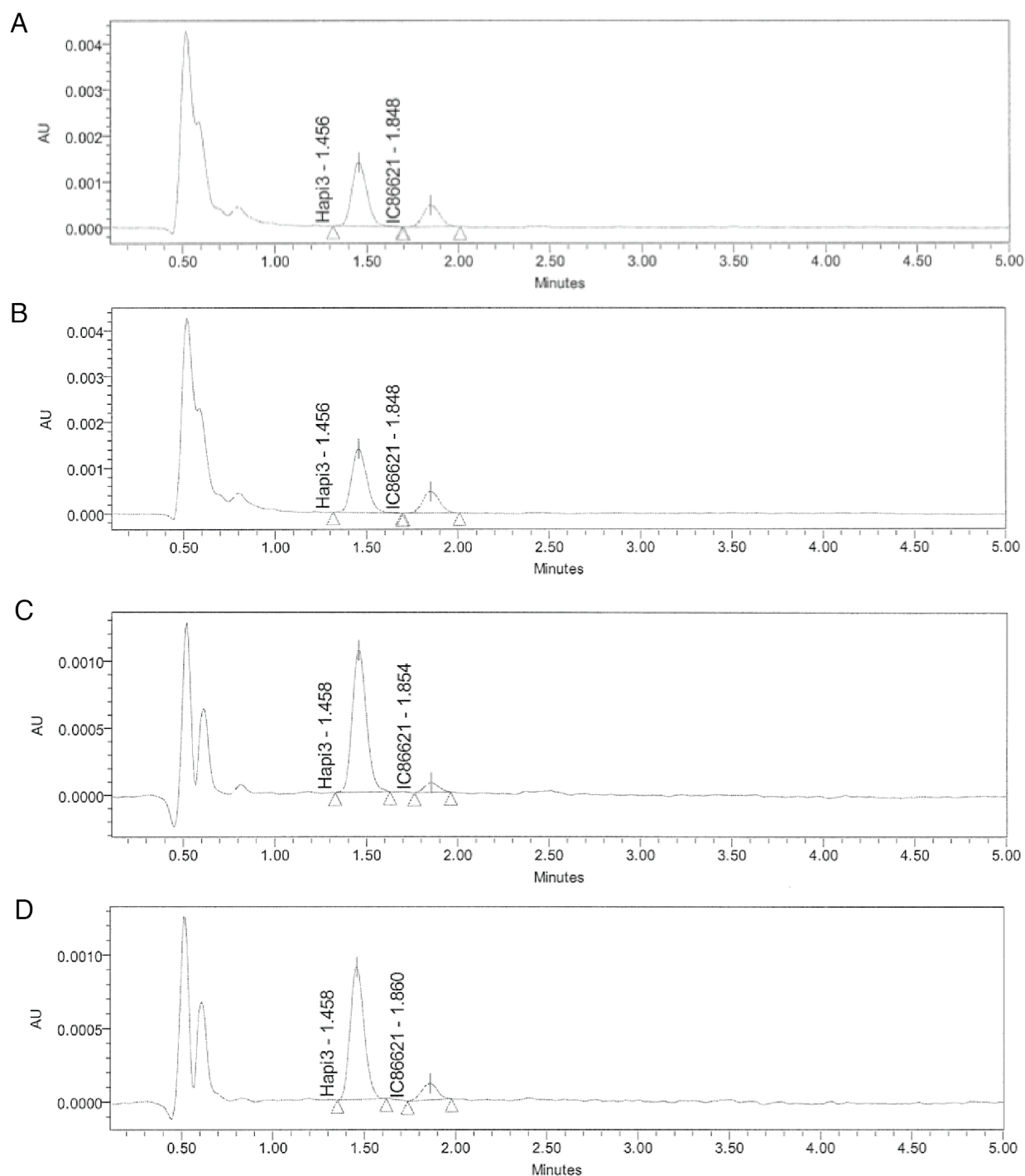


**Figure A3 HPLC chromatograms of kidney and brain extracts**

Chromatograms from resultant kidney and brain tissue extracts 4 h following p.o. administration of 814  $\mu\text{mol/L}$  Hapi3. All injections were performed as described in materials and methods section 2.2. A) Plasma, 320 nm. B) Plasma, 340 nm. C) Heart, 320 nm D) Heart, 340 nm. Unlabeled peaks are possibly unidentified metabolites. Hapi3 was detected at 320 nm, IC86621 was detected at 340 nm.